Necking of continental crust in magma-poor rifted margins: Evidence from the fossil Alpine Tethys margins

G. Mohn,[1] G. Manatschal,[1] M. Beltrando,[2] E. Masini,[1] and N. Kusznir[3]

Received 7 June 2011; revised 14 December 2011; accepted 21 December 2011; published 23 February 2012.

[1] Studies conducted in present-day magma-poor rifted margins reveal that the transition from weakly thinned continental crust (~30 km) in proximal margins to hyper-extended crust (≤10 km) in distal margins occurs within a narrow zone, referred to as the necking zone. We have identified relics of a necking zone and of the adjacent distal margin in the Campo, Grosina and Bernina units of the fossil Alpine Tethys margins and investigated the deformation and sedimentary processes associated with extreme crustal thinning during rifting. Within the basement rocks of the necking zone, we show that: (1) Grosina basement represents pre-rift upper/middle crust, while the underlying Campo unit consists of pre-rift middle/lower crust that was exhumed and cooled below ~300°C by ca. 180 Ma, when rifting started to localize within the future distal margin; (2) the juxtaposition of the Campo and Grosina units was accommodated by the Eita shear zone, which is interpreted as a decollement/decoupling horizon active at mid-crustal depth at 180–205 Ma; (3) the Grosina unit hosts a large-scale brittle detachment fault. Our observations suggest that crustal thinning, accommodated through the necking zone, is the result of the interplay between detachment faulting in the brittle layers and decoupling and thinning in ductile quartzo-feldspatic middle crustal levels along localized ductile decollements. The excision of ductile mid-crustal layers and the progressive embrittlement of the crust enables major detachment faults to cut into the underlying mantle, exhuming it to the seafloor. This structural evolution can explain the first-order crustal architecture of many present-day rifted margins.

Citation: Mohn, G., G. Manatschal, M. Beltrando, E. Masini, and N. Kusznir (2012), Necking of continental crust in magma-poor rifted margins: Evidence from the fossil Alpine Tethys margins, *Tectonics*, *31*, TC1012, doi:10.1029/2011TC002961.

1. Introduction

[2] The discovery of exhumed subcontinental mantle along Ocean-Continent Transitions (OCT) at present-day rifted margins focused most of the research on processes related to mantle exhumation. As a result, less attention has been paid to the processes leading to the extreme crustal thinning that predates mantle exhumation, resulting in the formation of hyper-extended domains (e.g., Exmouth plateau [*Driscoll and Karner*, 1998], West-African margin [*Aslanian et al.*, 2009; *Contrucci et al.*, 2004a], mid-Norwegian margin [*Osmundsen and Ebbing*, 2008]). In deep-water rifted margins, the final rifting phase is demonstrably accommodated by large offset, low-angle top-basement detachment faults, leading to the exhumation of continental crust and subcontinental mantle [e.g., *Whitmarsh et al.*, 2001]. *Manatschal et al.* [2001] and *Pérez Gussinyé and Reston* [2001] showed that when the detachment faults become active, continental crust is already brittle and thinned to less than 10 km. Moreover, the amount of visible extension accommodated by high-angle normal faults cannot account for the observed extreme crustal thinning [*Kusznir and Karner*, 2007; *Reston*, 2007]. Therefore major crustal thinning is unlikely to result from brittle, high-angle normal faulting alone. Observations from reflection and refraction seismic data show that crustal thickness decreases dramatically along the so-called necking zone. This zone separates weakly extended crust often preserving original crustal thickness (±30 km) at the proximal margin from hyper-extended crust (≤10 km) at the more distal margin [*Péron-Pinvidic and Manatschal*, 2009]. The strain distribution during crustal necking is at present poorly constrained mainly due to the lack of drill hole data from these zones and the limitations of seismic and other geophysical methods in revealing the nature of the rocks and deformation processes in the necking zones. Therefore we focused our study on well exposed remnants of the ancient Alpine Tethys margins preserved in the Bernina, Campo and Grosina units, in the European Alps. These units sample parts of the distal domain and the necking zone of the Mesozoic Adriatic rifted margin (see *Mohn et al.* [2010] for details on the restoration of the margin). They have been affected and reactivated by

[1]CNRS-EOST, Université de Strasbourg, Strasbourg, France.
[2]CNR-IGG, Turin, Italy.
[3]Department of Earth and Ocean Sciences, University of Liverpool, Liverpool, UK.

0278-7407/12/2011TC002961

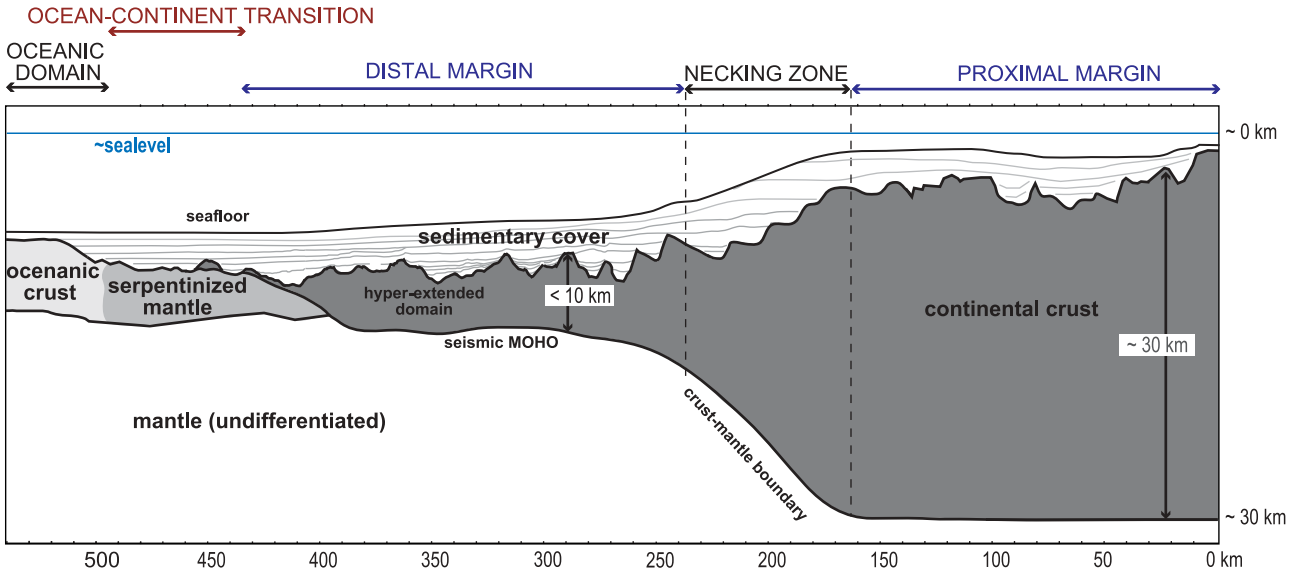

Figure 1. Idealized cross-section across a magma-poor rifted margin showing the different domains, crustal architecture and terminology used in this paper.

several deformations phases from the late Cretaceous onward during the Alpine orogeny. However, a detailed description of the Alpine evolution and restoration would go beyond the focus of this paper and was extensively investigated and discussed in previous works [*Mohn et al.*, 2010, 2011]. Despite Alpine tectonics, these units preserve evidence of a multistage rift-related evolution, which culminated in extreme crustal thinning in the Jurassic. The study presented here is aimed at (1) constraining the timing and distribution of crustal thinning along the margin, (2) detecting the structures leading to extreme crustal thinning and the conditions under which they were active and (3) defining the processes leading to extreme crustal thinning. In this paper we will present new structural, petrological and thermochronological data in order to constrain the crustal structure of this fossil necking zone. Based on these new data, we discuss the processes controlling crustal thinning and propose a coherent model to explain the structural and temporal evolution of Alpine Tethys margin.

2. Architecture of Magma-Poor Rifted Margins

2.1. Crustal Architecture of Present-Day Rifted Margins

[3] Although rifted margins show a large variability in their magmatic, structural and sedimentary evolution that may be related to their specific rift history and inheritance, most rifted margins worldwide share a remarkably comparable large-scale architecture. The domains defining the margin architecture are referred to as the proximal margin, the necking zone, the distal margin and the Ocean-Continent Transition (OCT) (Figure 1).

[4] Proximal margins are characterized by the occurrence of high-angle listric faults related to fault-bounded rift basins (e.g., North Sea [*Cowie et al.*, 2005, and references therein]) and β-factors typically less than 2, associated with limited crustal thinning (e.g., Jeanne d'Arc basin-Newfoundland margin [*Keen and de Voogd*, 1988; *Lau et al.*, 2006; *Van Avendonk et al.*, 2006]). Distal margins are characterized by hyper-extended crust that is separated from the oceanic crust by a domain of exhumed subcontinental mantle (OCT). *Manatschal et al.* [2001] and *Pérez-Gussinyé and Reston* [2001] demonstrated that low-angle normal faulting in the Iberia distal margin only started after the crust was thinned to less than 10 km. *Sibuet* [1992] and *Reston* [2007, 2009, and references therein] also showed that the amount of extension that can be inferred from imaged faults in distal margin is insufficient to explain the extreme crustal thinning to ~10 km. This observation, referred to as the 'extension discrepancy' [e.g., *Reston*, 2009] leads to the suggestion that the extreme crustal thinning recorded in the distal margin had to occur further continentward, prior to the activity of such faults.

[5] The necking zone is defined as the boundary between the proximal and distal margins, which undergo either little or extreme crustal thinning, respectively (Figure 1). Even if the style and architecture of necking zones may vary along strike, an abrupt crustal thinning can be recognized in many rifted margins. This thinning occurs over a relatively narrow area, which may be 50–60 km wide [e.g., *Osmundsen and Ebbing*, 2008]. The abrupt thinning is associated with a change in the Moho geometry from relatively flat in the proximal margin to a dip of up to 35° in the necking zone [*Lau et al.*, 2006]. The necking is generally best imaged by refraction seismic profiles and it has been recognized in the mid-Norway margin [*Olafsson et al.*, 1992; *Osmundsen and Ebbing*, 2008], the Goban Spur margin [*Bullock and Minshull*, 2005], the Armorican margin [*Thinon et al.*, 2002, 2003], the Iberia margin [*Whitmarsh et al.*, 1996; *Dean et al.*, 2000; *Zelt et al.*, 2003; *Afilhado et al.*, 2008], the Flemish Cap-Newfoundland-Nova Scotia margin [*Funck et al.*, 2003, 2004; *Lau et al.*, 2006; *Van Avendonk et al.*, 2006], the Moroccan margin [*Contrucci et al.*, 2004b; *Jaffal et al.*, 2009; *Klingelhoefer et al.*, 2009], the Angola margin [*Contrucci et al.*, 2004a; *Moulin et al.*, 2005; *Fernàndez et al.*, 2005], the Western Mediterranean Basin

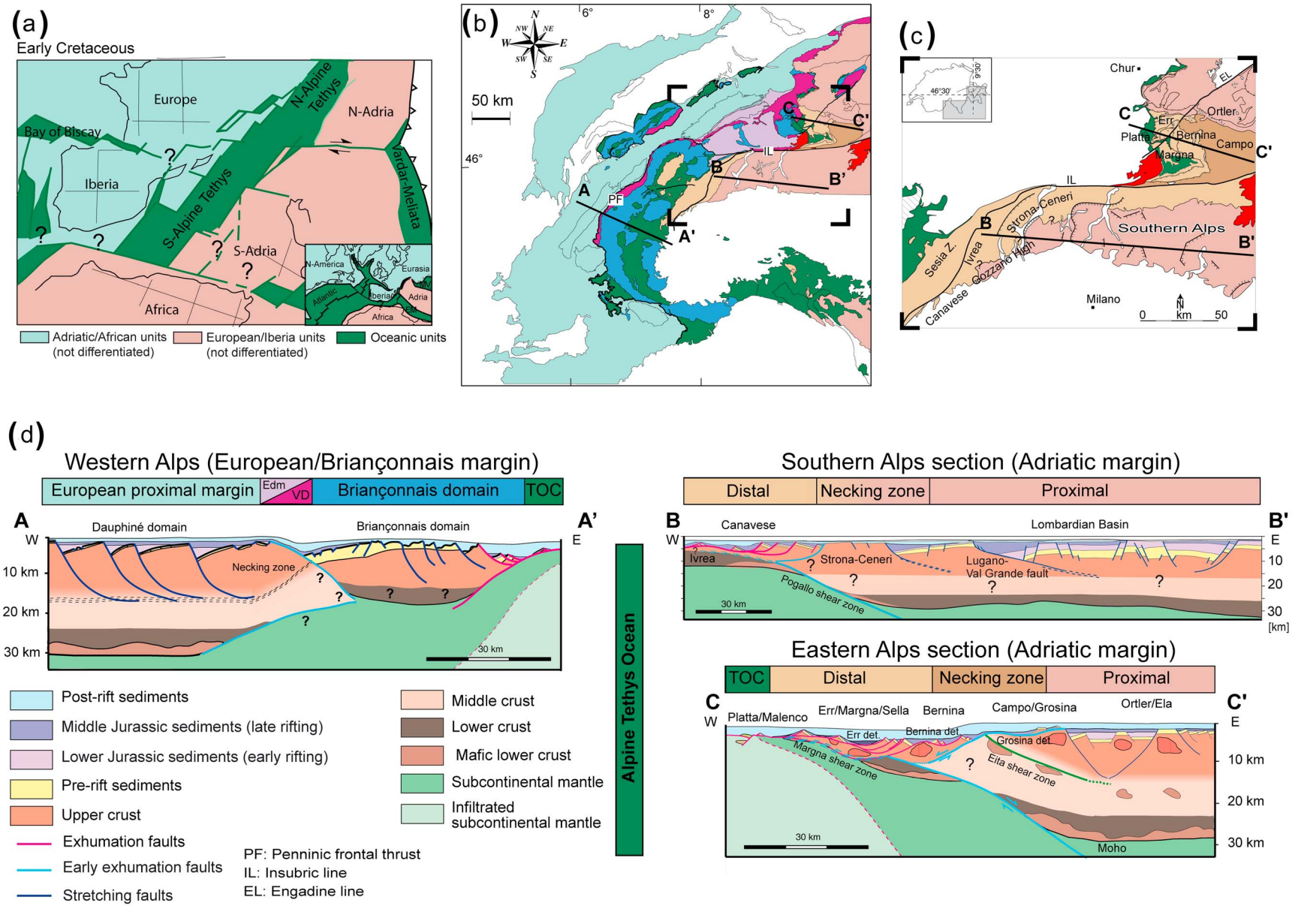
(a)
Early Cretaceous
Europe
N-Alpine Tethys
N-Adria
Bay of Biscay
Iberia
S-Alpine Tethys
Vardar-Meliata
S-Adria
Africa
N-America
Eurasia
Atlantic
Iberian
Adria
Africa
Adriatic/African units (not differentiated)
European/Iberia units (not differentiated)
Oceanic units
(b)
50 km
46°
6°
8°
A
A'
B
B'
C
C'
PF
IL
(c)
Chur
EL
Err
Ortler
Platta
Bernina
Campo
Margna
IL
Strona-Ceneri
Southern Alps
Sesia Z.
Ivrea
Canavese
Gozzano High
Milano
0 km 50
(d)
Western Alps (European/Briançonnais margin)
European proximal margin
Edm
VD
Briançonnais domain
TOC
Dauphiné domain
Briançonnais domain
Necking zone
10 km
20 km
30 km
Alpine Tethys Ocean
Post-rift sediments
Middle Jurassic sediments (late rifting)
Lower Jurassic sediments (early rifting)
Pre-rift sediments
Upper crust
Exhumation faults
Early exhumation faults
Stretching faults
Middle crust
Lower crust
Mafic lower crust
Subcontinental mantle
Infiltrated subcontinental mantle
PF: Penninic frontal thrust
IL: Insubric line
EL: Engadine line
Southern Alps section (Adriatic margin)
Distal
Necking zone
Proximal
Canavese
Lombardian Basin
Ivrea
Strona-Ceneri
Lugano-Val Grande fault
Pogallo shear zone
Eastern Alps section (Adriatic margin)
TOC
Distal
Necking zone
Proximal
Platta/Malenco
Err/Margna/Sella
Bernina
Campo/Grosina
Ortler/Ela
Err det.
Bernina det
Grosina det
Margna shear zone
Eita shear zone
Moho

Figure 2

[*Bache et al.*, 2010]; the Gulf of Aden [*Leroy et al.*, 2010] and the Gulf of California [*Lizarralde et al.*, 2007]. Within the necking zone, β-factors are typically >2 [*Reston*, 2009]. In conjugate pairs of rifted margins, necking zones are often characterized by symmetric geometries, in contrast to distal domains, which generally show a strongly asymmetric architecture [*Péron-Pinvidic and Manatschal*, 2009]. A recent study of *Osmundsen and Ebbing* [2008] has shown that necking zones recording significant crustal thinning prior to magmatic break-up can be identified even in magma-rich rifted margins.

2.2. Architecture of the Alpine Tethys Margins

[6] The Alpine Tethys rift system resulted from the separation of Africa and Adria from Europe and Iberia in Middle Jurassic time (Figures 2a and 2c). The opening was contemporaneous and kinematically linked with the opening of the Central Atlantic [e.g., *Ricou*, 1994]. Closure of the Alpine Tethys started in the Late Cretaceous and culminated in the collision between the European and Adriatic rifted margins in the Eocene/Oligocene [e.g., *Schmid et al.*, 1996; *Beltrando et al.*, 2010, and reference therein]. In the map in Figure 2, the distribution of the major paleogeographic Alpine units is shown together with 3 restored sections across (1) the European/Briançonnais margin (section A-A′); (2) the southern Adriatic margin (section B-B′); and (3) the northern Adriatic margin (section C-C′). The Adriatic proximal rifted margin is well exposed in the Lombardian Alps (section B-B′) and in the Upper Austroalpine nappe system (e.g., Ortler/Ela units in section C-C′). In all these units, Jurassic high-angle normal faults associated with half-graben basins have been described [*Bernoulli*, 1964; *Froitzheim*, 1988; *Conti et al.*, 1994]. These fault-bounded rift basins were active during initial rifting from late Triassic to Pliensbachian-Toarcian time. The distal margin is preserved in the Canavese-Ivrea zone (in section B-B′) and in the Lower Austroalpine nappe system (Bernina/Err/Margna/Sella units in section C-C′) (Figure 2). Relics of distal margin contain only pre-rift lower-crustal rocks (Malenco-Margna units, Ivrea zone) juxtaposed against pre-rift upper crust (Margna unit, Serie dei Laghi domain) along Jurassic shear zones (e.g., Margna shear zone) [e.g., *Bissig and Hermann*, 1999; *Müntener and Hermann*, 2001]. These observations suggest that 15–20 km of mid-crustal rocks have been excised during rifting. At the most distal edges of the rifted margin, the continental crust (Err and Bernina units, Canavese zone) and subcontinental mantle (Platta, Malenco units) are capped by low-angle top-basement detachment faults, which are associated with extensional allochthons [e.g., *Manatschal*, 2004; *Ferrando et al.*, 2004]. Extension related to final rifting in the distal margin and mantle exhumation in the OCT has been active from Pliensbachian to Callovian age [e.g., *Manatschal et al.*, 2007, and references therein]. The Mid-Ocean Ridge magmatic activity, within the northern Alpine Tethys domain, started during the Bathonian to Oxfordian, based on dating of the first post-rift sediments [*Baumgartner*, 1987] and U/Pb ages on zircons from first MORB-type gabbros [*Schaltegger et al.*, 2002].

[7] In the following part, we will mainly focus on the necking zone of the former Adriatic margin located between proximal and distal margins, which is preserved across the northern section (C-C′) in the Middle Austroalpine Campo-Grosina units (Figure 2d). However, because the northern and southern sections preserve different crustal portions of the fossil Adriatic rifted margin and were reactivated in a different way, we will use the southern section in the discussion to provide a more complete view of the architecture of the Adriatic rifted margin.

3. The Bernina and Campo-Grosina Domains

3.1. One Paleogeographic Position and Pre-Rift Geometry

[8] Along the northern section, relics of the Adriatic margin are preserved within the Austroalpine nappe system in SE-Switzerland and N-Italy (Figure 3). This nappe system was emplaced during Late Cretaceous west-directed shortening parallel to previous Jurassic extension (Figure 3). During this early stage of convergence, more proximal parts of the margin were thrust over more distal parts of the northern Adriatic margin resulting in the reactivation of former Jurassic rift structures (for a more detailed discussion see *Froitzheim et al.* [1994] and *Mohn et al.* [2011]). Of particular importance for this paper is the Alpine tectonic position of the Campo-Grosina and Bernina units. It is essential to note that the Alpine stacking did not modify the relative palaeogeographic position of the units relative to their position in the former Adriatic rifted margin. Therefore, in a restoration of the margin, the Bernina and Campo-Grosina units have to be placed in-between the Platta/Err units, preserving the Ocean Continent Transition, and the Ortler-Ela units, preserving remnants of the former proximal margin (Figure 3). *Mohn et al.* [2011], on the basis of detailed mapping, and structural, stratigraphic and petrological arguments, proposed that the Bernina and Campo-Grosina units preserve the transition between the former distal margin and the necking zone. In this context it is also important to note that the crystalline basement within the Austroalpine nappe stack is formed by rocks derived from the pre-rift Permian upper, middle, and lower crust as well as from the upper and lower mantle lithosphere, providing important constraints on the rift-related exhumation (Figure 3) [*Mohn et al.*, 2011]. Significantly, all these units

Figure 2. (a) Paleogeographic situation of the Alpine Tethys Ocean and adjacent margins during Early Cretaceous time [*Manatschal et al.*, 2011]. (b) Tectonic map of the Alps showing the distribution of the major palaeogeographic domains (modified after *Schmid et al.* [2004]). (c) Geological overview of the Eastern and Southern Alps modified after *Bernoulli et al.* [1990] and *Manatschal and Bernoulli* [1999]. (d) Reconstructed palaeogeographic sections across the European/Briançonnais and Adriatic rifted-margins, European/Briançonnais transect (section A-A′ modified after *Lemoine et al.* [1986] and *Mohn et al.* [2010]), Southern Alps transect (section B-B′ modified after *Bertotti et al.* [1993] and *Handy et al.* [1999]) and Eastern Alps transect (section C-C′ modified after *Froitzheim and Manatschal* [1996] and *Mohn et al.* [2010]) (for traces of sections see maps above).

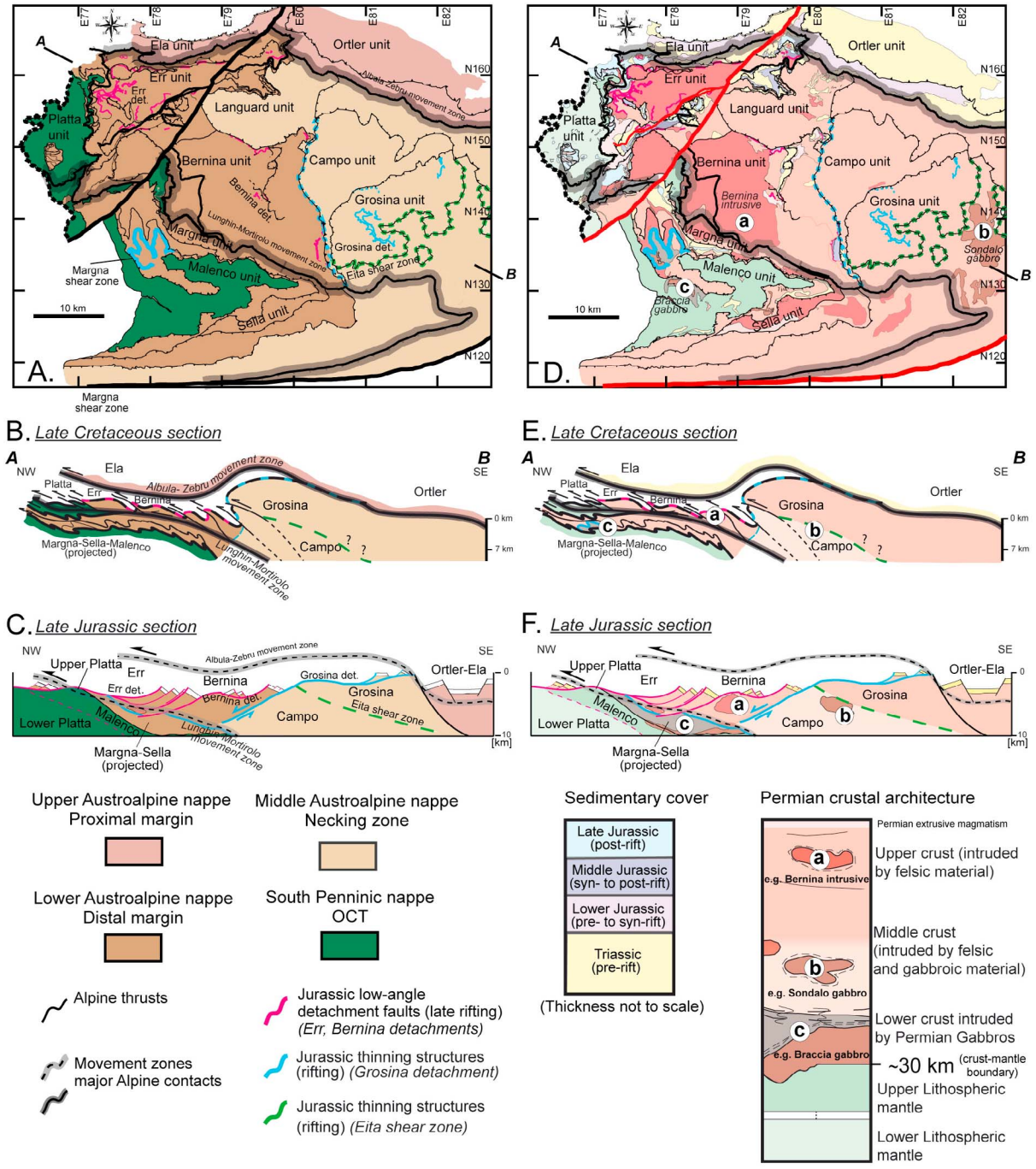

Figure 3. (a) Map showing the paleogeographic domains of the Austroalpine and Upper Penninic nappe systems in SE Switzerland and N-Italy. (b) Late Cretaceous section showing the distribution of paleogeographic units of the former Adriatic rifted margin after the west-directed convergence (modified from *Mohn et al.* [2011]). (c) Late Jurassic architecture of the Adriatic (Austroalpine) rifted margin showing the initial position of the paleogeographic units (modified from *Mohn et al.* [2010]). (d) Lithological map of the Austroalpine and Upper Penninic nappe systems in SE Switzerland and N-Italy. (e) Late Cretaceous section showing the reactivation of the former Adriatic rifted margin during the D1 west-directed convergence (modified from *Mohn et al.* [2011]). (f) Late Jurassic crustal architecture of the Adriatic (Austroalpine) rifted margin (modified from *Mohn et al.* [2010]). The section to the bottom right shows a simplified cross section of Permo-Jurassic cover associated with a cross-section through the crust in later Permian time, indicating the original position of the rocks found today in the different tectonic units (after *Mohn et al.* [2011]). Note that the Albula-Zebru and Lunghin-Mortirolo movement zones are major Alpine discontinuities inherited from the Jurassic rifting (for further details see *Mohn et al.* [2011]). Coordinates given in the maps refer to the Swiss grid.

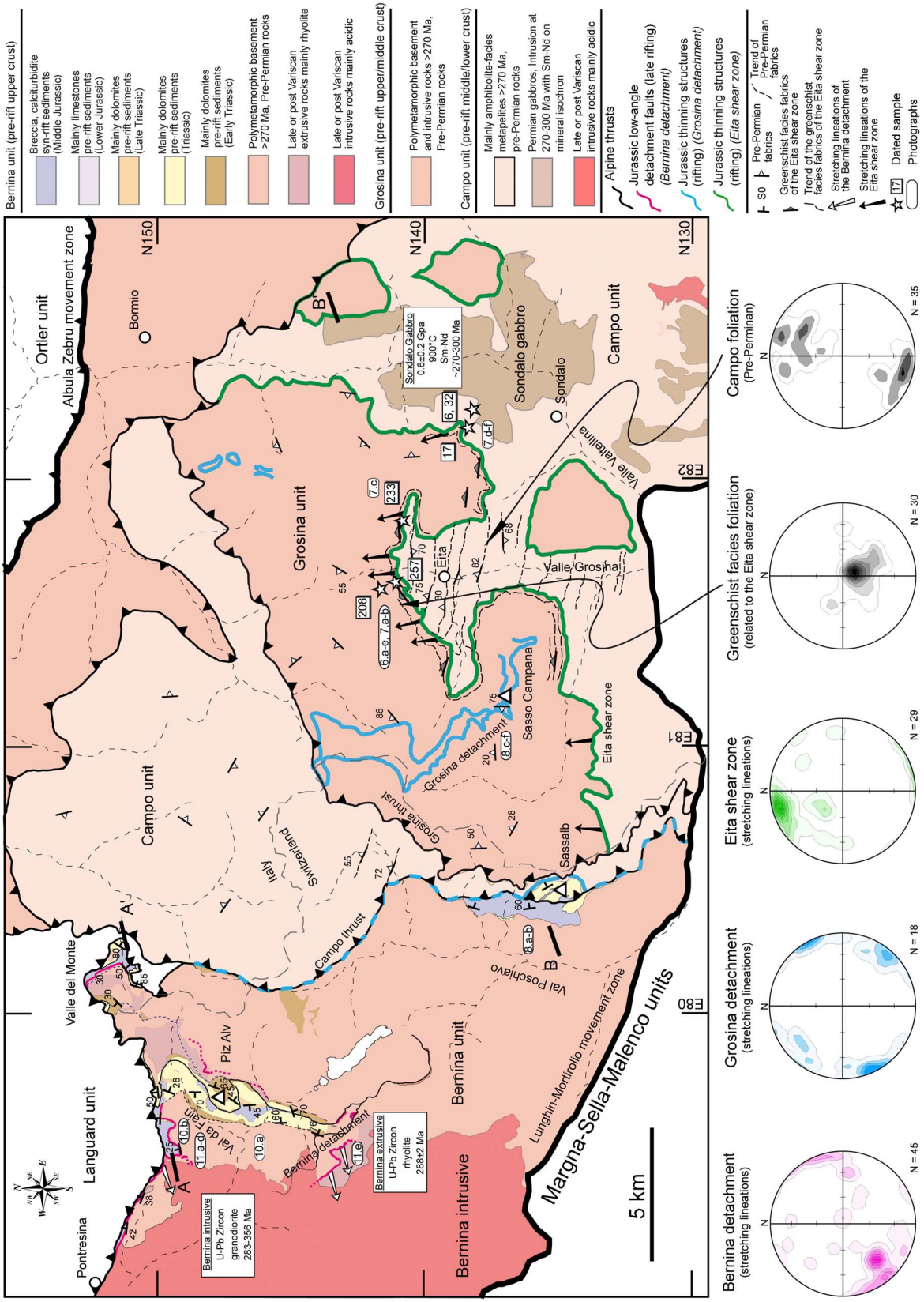

Figure 4. Geological map of the Bernina-Campo-Grosina units in SE-Switzerland and N-Italy. Map compiled from *Staub* [1946], *Bonsignore et al.* [1969], *Montrasio et al.* [1969], *Meier* [2003], and our own observations. Orientations of structural elements in the study area are presented in Lower hemisphere Schmidt projection. Note that localization of photographs of the Figures 6, 7, 8, 10, and 11 and $^{40}Ar/^{39}Ar$ samples (Figure 9) are indicated on the map as well as the trace of the cross sections of Figure 5.

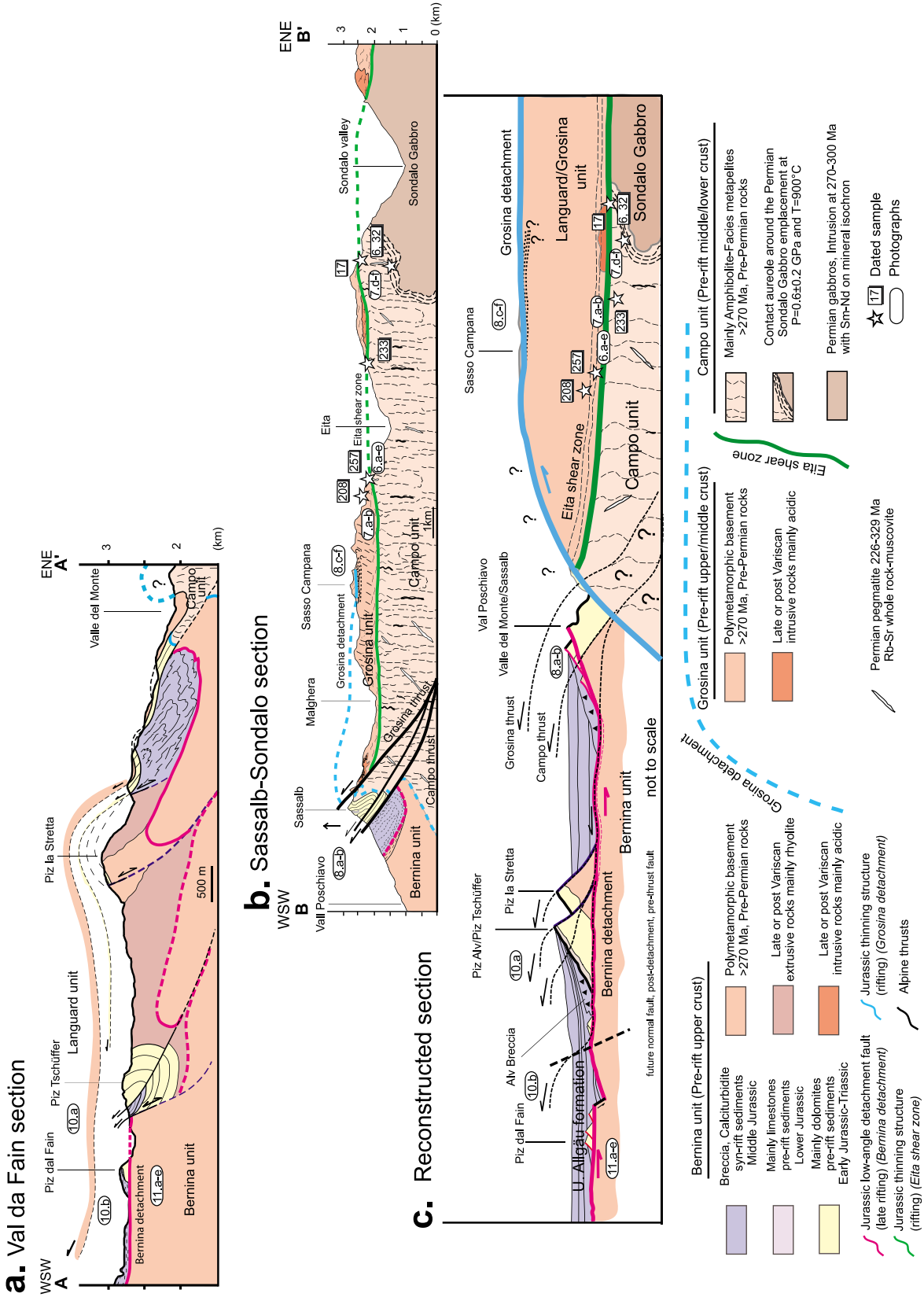

Figure 5. Geological sections across (a) Val dal Fain and (b) Sassalb–Sondalo and (c) restored section showing the pre-Alpine structures and their relation to the sediments and basement rocks in the Bernina, Campo-Grosina units. Localization of the cross-sections is shown in Figure 4 (modified after *Mohn et al.* [2011]). Note that localization of photographs of the Figures 6, 7, 8, 10, and 11 and $^{40}Ar/^{39}Ar$ samples (Figure 9) are indicated on the cross-sections.

preserve primary contacts with pre-, syn- or post-rift Mesozoic sediments and were located within the uppermost crust at the beginning of convergence [*Mohn et al.*, 2011, and references therein] (Figure 3). Therefore exhumation of the various crustal levels had to occur before onset of Alpine deformation but after Permian time, since the petrographic evolution of pre-rift lower crustal rocks indicates that they underwent near-isobaric cooling, with no evidence for significant crustal thinning during Permian to Triassic time [*Müntener et al.*, 2000]. Therefore, in this area, the continental crust was equilibrated at 30 km before the onset of Jurassic rifting [*Müntener et al.*, 2000].

3.2. Alpine Evolution

[9] Any attempt to reconstruct the pre-Alpine rift-related history depends on the ability to distinguish between Alpine and pre-Alpine structures: a subject that has been discussed extensively by *Mohn et al.* [2011]. In this section we will briefly summarize the Alpine evolution of the Bernina and Campo-Grosina units (Figures 4 and 5).

[10] Alpine deformation structures in the Bernina and Campo-Grosina units are largely restricted to a few, well-localized top to the NW thrust faults that are associated with duplex structures and NW facing anti- and syn-formal fault bend folds with NE-SW trending axes (Figure 5). The Campo basement is thrusted over the underlying Bernina unit along the Campo thrust fault (Figure 5). The contact between the overlying Grosina and the underlying Campo unit is marked by the Grosina thrust fault in Val Poschiavo [*Staub*, 1946] (Figure 5). Deformation along the Grosina thrust is localized along a narrow (∼m), lower greenschist facies shear zone with stretching lineations defined by elongated feldspar and asymmetric strain fringes around K-feldspar porpyroclasts indicating a top to the west sense of shear, interpreted as related to a Late Cretaceous Alpine thrust fault (Figures 4 and 5) [*Staub*, 1946; *Mohn et al.*, 2011]. Further to the east, in Valle Grosina, the Campo and Grosina basement units are juxtaposed along a major structure referred to as the Eita shear zone (Figures 4 and 5) [*Meier*, 2003]. *Meier* [2003] interpreted this shear zone as a Late Cretaceous Alpine thrust representing the continuation of the Grosina thrust further to the east, an interpretation that is not in line with the results presented in this paper. Indeed, in Val Poschiavo the late Cretaceous Grosina thrust truncates the Eita shear zone, suggesting that the latter structure is older.

[11] Locally, at Sassalb, in Val Poschiavo, the Mesozoic cover sequence of the Bernina unit, which now forms a W-facing synform, is directly juxtaposed against Campo basement along a pre-Alpine brittle structure referred to as the Grosina detachment. This contact is truncated by the Late Cretaceous thrust faults (Campo and Grosina thrusts), which support the pre-Alpine age of this structure, and is interpreted to truncate the Eita shear zone (Figure 5) [*Mohn et al.*, 2011]. Our study shows that the Alpine overprint is moderate and the Alpine displacement along the Campo and Grosina faults is minor (Figure 5). In the Bernina unit in the Val dal Fain section, it can be shown that thrust faults nucleate along a pre-existing rift-related detachment fault referred to as the Bernina detachment (Figure 5a). Thrust faults are forming imbricate and/or duplex structures, which are further complicated by the existence of small extensional allochthons and/or the existence of rift-related high-angle normal faults (for details see *Mohn et al.* [2011]).

4. Rift-Related Structures in the Campo-Grosina Units

4.1. Campo and Grosina Basement: Petrological Observations

[12] The Campo-Grosina units preserve a 3 km thick crustal section that is exposed to the south and the east of the Swiss-Italian border together with few slices of Mesozoic cover (Figures 4 and 5). In Valle Grosina, the Campo basement is separated from the overlying Grosina basement by the Eita shear zone [*Meier*, 2003] (Figures 4 and 5).

[13] The Campo basement consists mainly of metapelites, locally associated with amphibolites and silicate-bearing marbles, which show a multiphase pre-Alpine tectonic history [*Meier*, 2003]. In this study, we will mainly focus on the Campo basement exposed in the Valle Grosina (Figure 4). In this area, the most common metamorphic fabric visible in the field is generally a steeply dipping, E-W striking foliation (Figure 6a and 6b). In the micaschists, this fabric is defined by a foliation containing muscovite-biotite-plagioclase-quartz ± garnet ± staurolite ± sillimanite, which formed at temperatures between 550 and 650°C [*Bucher and Frey*, 1994; *Meier*, 2003]. Similar metamorphic assemblages have been reported by *Notarpietro and Gorla* [1981], *Braga et al.* [2001], and *Meier* [2003] indicating a regional metamorphic equilibration under amphibolite facies conditions. The absolute timing of formation of the sillimanite-bearing foliation of the Campo unit is unknown. However, similar metamorphic conditions were reached in the adjacent Oetztal basement and the South Alpine basement at ca. 320–340 Ma [*Boriani and Villa*, 1997; *Thöni*, 1999].

[14] The amphibolite-facies Campo basement in the Valtellina valley underwent local contact metamorphism during the intrusion of the Sondalo gabbroic complex, dated at ca. 270–300 Ma (Permian; Figure 4) [*Tribuzio et al.*, 1999]. *Tribuzio et al.* [1999] and *Braga et al.* [2001, 2003] proposed that the Sondalo gabbro was emplaced at P = 0.6 ± 0.2 GPa and T = 900°C, at mid-crustal depth. Contact metamorphism is pervasive within a 20 to 30 m thick aureole, which preserves abundant evidence of partial melting of the metapelites with extraction of peraluminous anatectic melts and crystallization of granitoid pods [*Braga et al.*, 2001]. Locally, migmatitic banding developed concordant with the regional, steeply dipping foliation of the metapelitic rocks. Migmatization is generally restricted to narrow belts, which do not exceed the thickness of a few tens of meters surrounding the intrusion. The Campo basement was also intruded by more Si-rich magmas, leading to the formation of granite, granodiorite and pegmatite dykes, which are all discordant with respect to the pre-Permian Campo fabrics (Figure 6b). Acid magmatism has been dated by Rb-Sr method on muscovite-whole rock. Granitoids yielded Permian ages between 282 ± 4 Ma and 259 ± 4 Ma [*Del Moro and Notarpietro*, 1987; *Meier* 2003, and references therein] while pegmatites are showing a wider age range between 329 and 226 Ma [*Hanson et al.*, 1966; *Thöni* 1981]. More recently *Sölva et al.* [2003] dated a magmatic garnet from a pegmatite with the Sm/Nd method, for which they obtained Permian crystallization ages of 255.4 ± 2.8 Ma and 250 ±

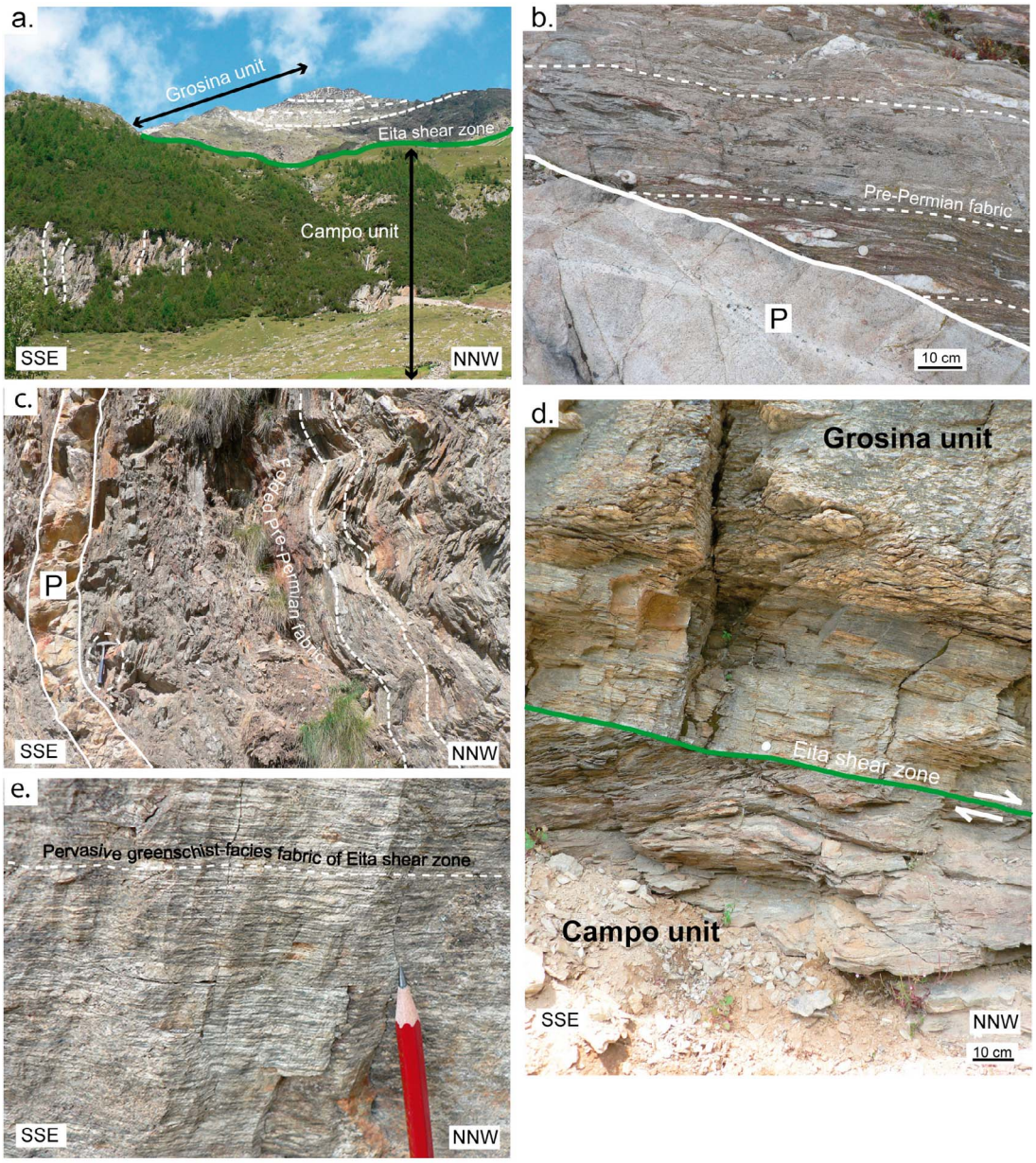

Figure 6. Field photographs showing the structural elements of Campo, Grosina units and Eita shear zone in Valle Grosina near Eita (for the location of photographs see Figures 4 and 5). (a) Large scale structures observed in Valle Grosina: note the angular discordance between the steep Pre-Permian Campo fabric and the flat pervasive greenschist pervasive foliation linked with the Eita shear zone (in green) within the Grosina basement (816305/139771). (b) Amphibolite-facies metapelites of the Campo unit crosscut by Permian pegmatite (P) (816315/139716) (c) In the vicinity of Eita shear zone, the pre-Permian Campo fabric associated with Permian dykes display recumbent folds (816467/141107). (d) Contact between Campo and Grosina basement formed by the Eita shear zone; note the drag of the Campo fabric due to the shearing indicating a top to NNW sense of shear (816481/141150). (e) North-dipping pervasive greenschist facies fabric related to the Eita shear zone (816510/141280). Coordinates are given with the Swiss grid.

2.7 Ma from the core and the rim respectively. The polyphase magmatic evolution of the Campo unit is coherent with similar observations from other Alpine basement terrains, which preserve abundant evidence of a major prerifting Permian magmatic event in all crustal levels [*Rebay and Spalla*, 2001; *Schuster and Stüwe*, 2008, and references therein].

[15] The Grosina basement is mainly made up of Paleozoic rocks, which have undergone several phases of pre-Alpine deformation. Like the Campo basement, it is characterized by amphibolite facies metamorphic assemblages, as indicated by the occurrence of sillimanite-biotite gneiss associated with garnet-biotite-staurolite micaschists, minor diopside-bearing calc-silicates, andalusite bearing micaschists and variably

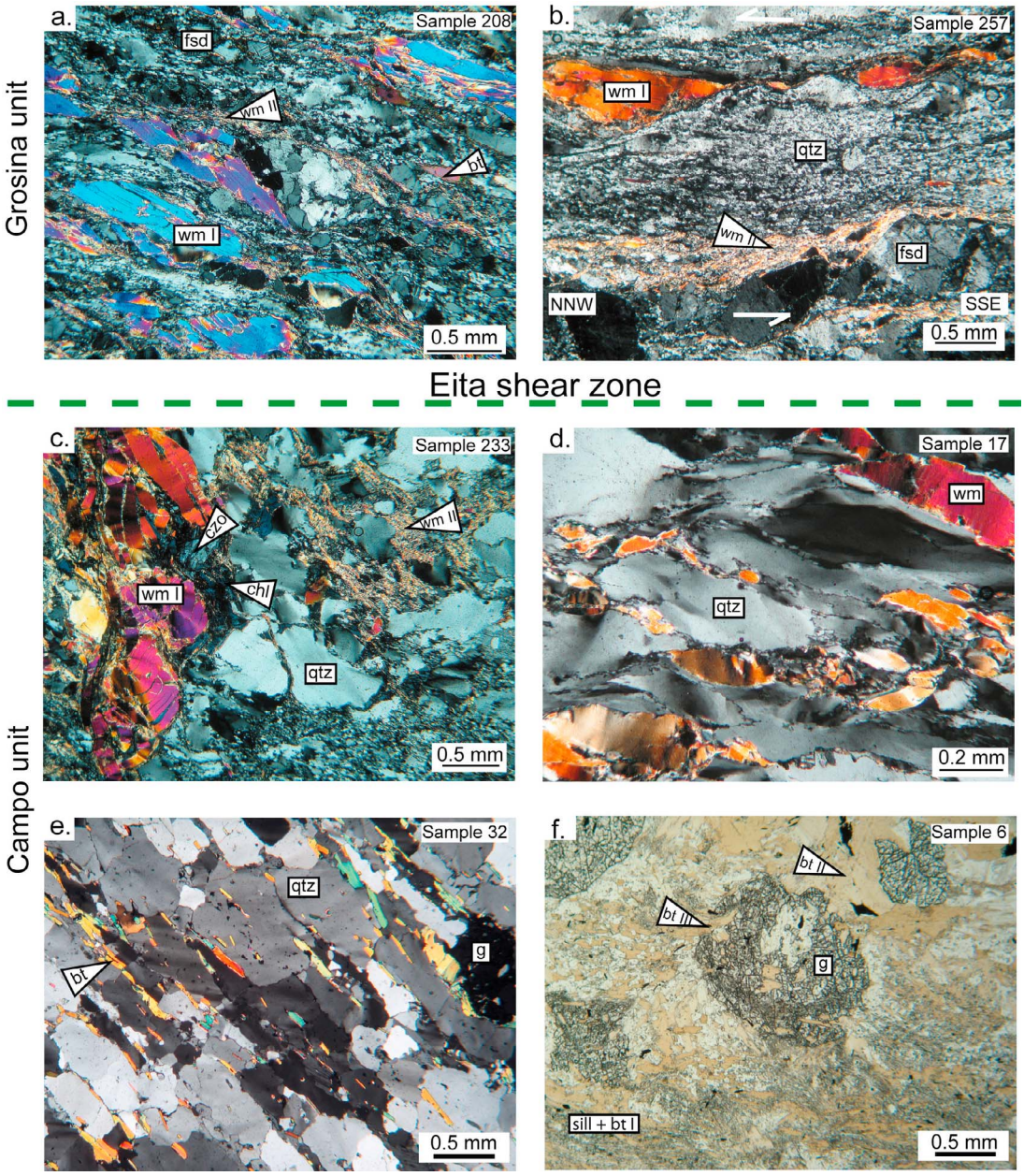

Figure 7. Photomicrographs of the samples that have been dated in this study. Pervasive greenschist fabric related of the Eita shear zone within the Grosina basement located respectively at (a) 100 m (816515/141332) and (b) 1 m (816481/141150) from the contact between the Grosina and Campo units. In Figure 7b, sense of shear can be determined along C′-type shear bands indicating a top the NNW sense of shear. (c) Deformed and retrogressed pegmatite dyke located in the Campo basement in the immediate vicinity (∼1 m) of the contact with the Grosina basement (816489/141128). (d) Quartz mylonite associated with deformed white mica (822042/138708). (e) Banded migmatite at about 30 m from the Permian Sondalo gabbro within the contact aureole (822096/138665). (f) Migmatite characterized by a compositional banding sampled within the contact aureole of the Permian Sondalo gabbro (822574/138236). Coordinates are given with the Swiss grid. Mineral abbreviations are as follows: bt, biotite; chl, chlorite; czo, clinozoisite; fsd, feldspar; g, garnet; qtz, quartz; sill, sillimanite; wm, white mica. For the location of photographs see Figure 4 and 5.

deformed biotite orthogneiss [*Staub*, 1946; *Koeing*, 1964; *Schudel*, 1965; *Meier*, 2003]. Locally granodioritic intrusions can be described crosscutting previous amphibolite facies foliation of the country rocks.

4.2. Eita Shear Zone

[16] The Eita shear zone, as defined by *Meier* [2003], can be mapped continuously over more than 20 km (Figure 4), residing at the same structural level separating the Campo

from the Grosina basement. This contact is well exposed in the Valle Grosina close to the village of Eita (Figures 4, 6a, and 6d). North of Eita, within thirty meters from the main contact, the typical steep Campo fabric is progressively overprinted by later deformation, leading to recumbent folds with E-W trending fold axes and a shallow W-dipping axial plane (Figure 6c). A finite strain gradient is observed approaching the contact. This is best shown by the amplitude of recumbent folds associated with the rotation of the Campo fabric due to shearing along the Eita shear zone. Locally, Permian pegmatites are folded in the vicinity of the shear zone, indicating that shearing must post-date their intrusion (Figure 6c). Microstructural observations reveal that the amphibolite-facies Campo fabric is dynamically retrogressed to greenschist facies conditions, as indicated by the break down of biotite to chlorite and destabilization of garnet and sillimanite into chlorite and white mica. At the contact with the underlying Campo unit, the Grosina basement is overprinted by a north-dipping flat fabric related to the Eita shear zone, which affects the Grosina orthogneiss for up to 200 m (Figures 4 and 6e). Up section, the transition between the flat-lying fabric domain and the less deformed Grosina orthogneiss remains weakly constrained. This shear fabric is defined by quartz + white mica II + chlorite + illmenite wrapping around porphyroclastic K-feldspar, plagioclase and white mica I (Figure 7a, 7b, and 7c). Relics of porphyroclasts of quartz display a core and mantle structure with evidence of bulging recrystallization. Newly recrystallized fine-grained quartz is characterized by a strong shape preferred orientation oblique with respect to the shear plane characteristic of subgrain rotation recrystallization (Figures 7a and 7b). K-feldspar and plagioclase, on the contrary, are fractured and transected by microfaults indicating a brittle behavior (Figure 7b). Large (1 mm) fractured and kinked white mica I is oriented parallel to the mylonitic fabric defined by white mica II and chlorite (Figure 7a). Locally, moving away from the Campo/Grosina interface, green biotite can be found as pseudomorphs on porphyroclastic white mica I (Figure 7a). The occurrence of static, post kinematic growth of secondary chlorite is commonly observed. These observations indicate that from the contact with the Campo basement for a thickness of 200 m within the Grosina basement, pre-Alpine high-T fabrics as well as granodioritic intrusions are dynamically re-equilibrated at greenschist facies metamorphic conditions related to the Eita shear zone [*Meier*, 2003]. Stretching lineations defined by elongated K-feldspar porpyroclasts dip gently to the NNW. Shear bands, mica fish, and asymmetric strain fringes around K-feldpars indicate a top-to-the NNW sense of shear (Figures 6d and 7b,). The evidence of brittle deformation of feldspar, associated with the growth of chlorite, white mica and the dynamic recrystallization of quartz suggest that shearing occurred in the temperature range between 300 and 400°C. Further to the west, the presence of green-brown biotite in the shear fabric, together with microstructural evidence of grain boundary migration in quartz, has been taken as an indicator that shearing had to occur at temperatures around 400°C [*Meier*, 2003].

4.3. Grosina Detachment

[17] The Grosina basement at Sasso Campana exposes the best-preserved section across the Grosina detachment. In this locality at least two well-developed, spectacularly exposed sub-horizontal brittle fault zones can be mapped (Figures 4, 5, 8c, and 8d). The lower brittle fault zone consists of a continuous, less than 10 m thick horizon, which can be followed over a distance of more than 8 km (Figure 4). Locally, a second fault zone can be mapped. This second fault may either represent a branch of a second detachment fault that was cut by the first one (see incisement structures of *Lister and Davis* [1989]) or may represent an anastomozing fault belonging to the same detachment system. The detachment faults consist of cataclastic fault rocks showing angular clasts and transgranular fractures passing upwards into phyllosilicate-rich gouge (Figures 8d and 8f). No crystal plastic or dynamic recrystallization of quartz can be observed along the Grosina detachment fault, indicating that these fault zones were active at temperatures lower than 300°C. Stretching lineations are poorly defined and are highly variable, showing either NW-SE or NE-SW trends (Figure 4). The general lack of kinematic indicators hinders the determination of sense of shear. At the top of the Grosina basement, the detachment fault locally crosscuts quartz mylonites (Figure 8e). These quartz mylonites can also be observed as clasts in the cataclasites and gouges defining the Grosina detachment (Figure 8f). The mylonitic shear zone is 20 to 30 m wide and is discordant to the Grosina fault zone. The angle between the fault zone and the mylonite shear zone is approximately 20°. The shear zone is discontinuous and shows a anastomozing geometry. The quartz mylonites are formed by quartz + chlorite + illmenite, while plagioclase and K-feldspar and white mica are preserved as porphyroclasts (Figure 8e). Fine-grained aggregates of quartz crystals display a strong lattice preferred orientation associated with a pervasive dynamic recrystallization dominated by subgrain rotation mechanism (Figure 8e). Thus, the evidence of brittle deformation affecting porphyroclastic feldspar as well as the mechanism of quartz recrystallization constrain the temperature condition for the activity of this shear zone between 350°C and 400°C. Locally, the foliation is also defined by fine aggregates of white micas. A NE-SW stretching lineation defined by elongated K-feldspar porphyroclasts is observed in the quartz mylonite. From shear band and mica fish structures a top to the NE sense of shear can be inferred for this mylonitic shear zone. Based on field relations, it is not clear whether the quartz mylonite represents a previous phase of deformation related to the detachment fault or whether it represents an independent older structure. At the moment no age constrains are available for these mylonites. Further to the west at Sassalb (Figures 8a and 8b), the contact between Triassic dolomites belonging to the Bernina unit and the Campo basement is marked by a brittle fault zone. Along the contact characteristic brittle fault rocks, similar to those found at the top of the Grosina basement can be found.

5. Geothermochronology of Campo Basement and Eita Shear Zone

5.1. The $^{40}Ar/^{39}Ar$ Geochronology of the Campo Basement

[18] Two samples were collected from the country rock of the Sondalo gabbroic intrusion in order to constrain thermal evolution and exhumation history of the Campo basement.

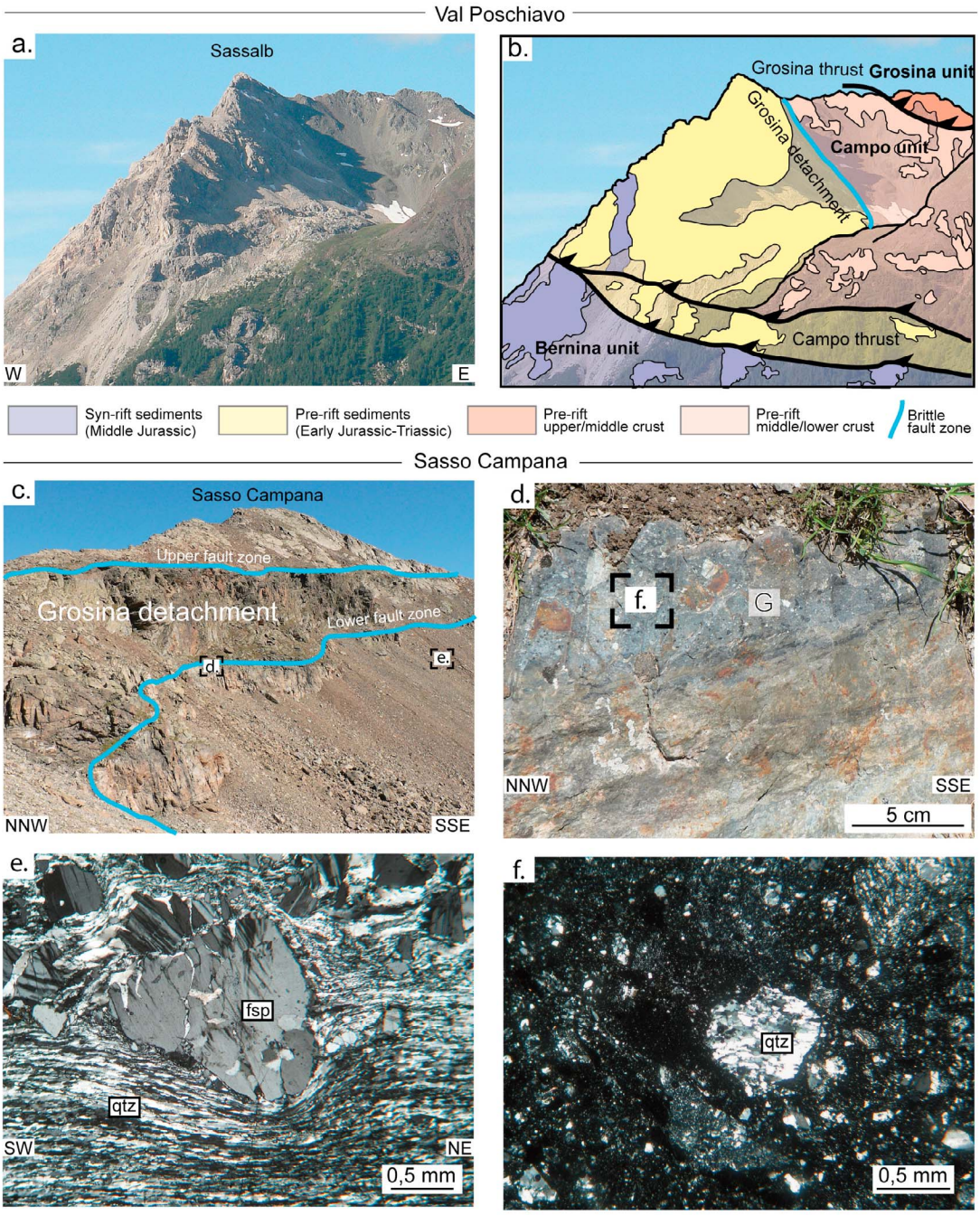

Figure 8. (a) Photograph and (b) line drawing from the Val Poschiavo at Sassalb showing the contact between Campo-Grosina and Bernina units. Campo unit is juxtaposed against the Bernina unit along a pre-Alpine contact referred to as Grosina detachment (in blue) crosscut by the Grosina and Campo thrust faults. Note that the photograph has been inverted to be compared with the map (Figure 4) and cross-section (Figure 5b) (804796/134771). (c) Grosina detachment at the top of Grosina unit in Sasso Campana. Note that two splays of the detachment can be observed (811306/137391). (d) Gouge zone as exposed along the Grosina detachment (811316/137314). (e) Photomicrographs of quartz mylonite from a shear zone crosscut by the Grosina detachment. Note the dynamically recrystallized quartz flows around the feldspar clast (811311/137194). (f) Photomicrographs of clast of quartz mylonite within a gouge from the Grosina detachment (811316/137314). Coordinates are given with the Swiss grid. For the location of photographs see Figure 4 and 5. (For mineral abbreviations see caption of Figure 7).

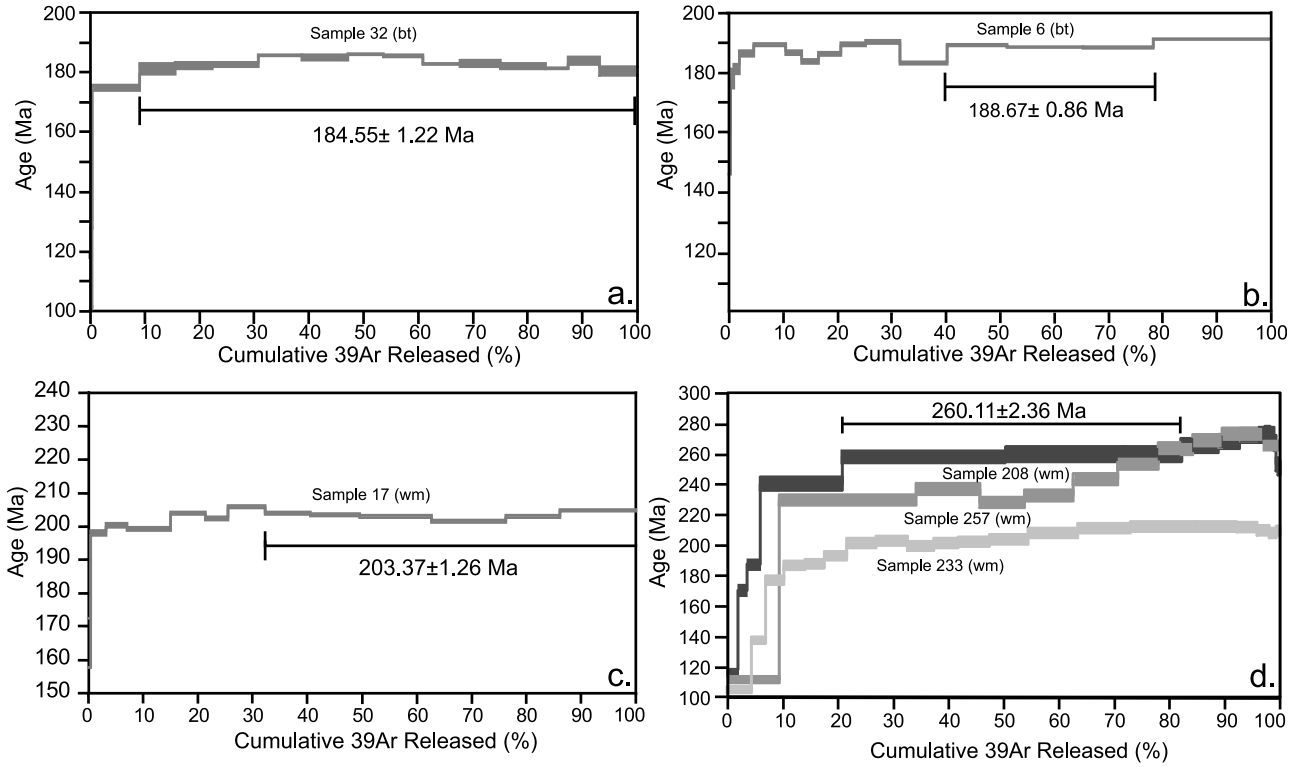

Figure 9. (a–d) The $^{40}Ar/^{39}Ar$ step-release spectra. For location of dated samples see Figures 4 and 5; for the GPS coordinates of the samples see Tables S1 and S2. Mineral abbreviations are as follows: bt, biotite; wm, white mica. For discussion see text.

Samples for $^{40}Ar/^{39}Ar$ geochronology were taken from the migmatites and quartzo-feldspathic dykes within the contact metamorphic aureole of the Sondalo Gabbro. Samples were crushed, sieved, cleared by ultrasound and then passed through the Frantz Magnetic separator. Hand-picking was made under the binocular microscope choosing the 250–500 μm size fraction. Details of the method and analytical data are given in the auxiliary material, and sample locations are given in Figures 4 and 5 and in the auxiliary material.[1]

[19] Sample 32 was collected in a banded migmatite at about 20 m from the gabbro-country rock contact. This rock is characterized by the presence of one foliation defined by white mica and biotite, which are in equilibrium with quartz + garnet + plagioclase (Figure 7e). The biotite-bearing foliation is also found within quartz porphyroblasts, suggesting that the formation of the fabric was followed by grain size coarsening of the quartzitic matrix. Irregular and lobate boundaries associated with variable grain size of quartz crystals indicate recrystallization by high-temperature grain boundary migration. Local retrogression of biotite to chlorite is observed. Only one generation of biotite could be observed in this sample on microstructural ground (Figure 7e).

[20] Sample 32 yielded a relatively flat apparent age spectrum, starting from an initial age of 174 Ma, increasing progressively to 186 Ma and then decreasing to 180 Ma. Over 91% of the ^{39}Ar gas release occurred between steps 2 and 15, ranging from 179 to 185 Ma (Figure 9a).

[21] Sample 6 was collected from a leucocratic layer of a migmatite characterized by compositional banding. Thin, spaced layers made of fine-grained aggregates (~0.1 mm) of sillimanite, biotite I and quartz define a weak anastomozing foliation concordant with the foliation in the metapelitic country rocks (Figure 7f). Porphyroblastic garnet is found exclusively in the leucosome, with inclusions of biotite I and quartz. Garnets are associated with a second generation of large biotite II (Figure 7f). Coarse anhedral quartz and subhedral plagioclase grains are also found. A younger generation of fine-grained (~0.3 mm) biotite III is present in cracks of the garnet (Figure 7f). Thus, at least three different generations of biotite could be identified in this rock based on microstructural observations.

[22] The apparent age spectrum of sample 6 is slightly more complex than for sample 32. Steps 1 to 11 yielded apparent ages in the 178–190 Ma range and are followed by a relatively flat part of the spectrum between steps 12 and 15, yielding ages in the 188 Ma range with 59% of the total ^{39}Ar released (Figure 9b).

5.2. The $^{40}Ar/^{39}Ar$ Geochronology of the Eita Shear Zone

[23] Two samples (208, 257) were collected for $^{40}Ar/^{39}Ar$ dating on white mica at the base of the Grosina basement affected by greenschist-facies shear fabric. Samples 208 and 257 have been taken respectively at ~100 m and ~1 m from the contact with the underlying Campo unit. Detailed methods and analytical data are given in the auxiliary material, and sample locations in Figures 4 and 5 and the auxiliary material.

[1]Auxiliary materials are available in the HTML. doi:10.1029/2011TC002961.

[24] Sample 208 is an orthogneiss located within the Grosina basement at ~100 m from the contact with the Campo basement (Figure 4). This sample is characterized by a pervasive fine-grained shear fabric containing white mica II + green biotite + recrystallized quartz wrapping porphyroclasts (1.2–0.2 mm) of K-felsdspar, plagioclase white mica I and relict quartz (Figure 7a). The mineral assemblage marking the shear fabric indicates that it formed under greenschist facies conditions.

[25] Sample 208 yielded an age spectrum that increases from an initial apparent age of ~119 Ma to a relatively flat section between steps 5–7 (61% of the total ^{39}Ar released) in the 256–263 Ma range (Figure 9d). These steps are followed by apparent ages that increase slightly and then decrease with the final ~20% gas released (Figure 9d).

[26] Sample 257 is an orthogneiss collected in the Grosina basement at ~1 m from the contact between Campo and Grosina (Figure 4). The observed main fabric is similar to the greenschist facies foliation described in sample 208. The fine-grained shear fabric is defined by white mica II + quartz + chlorite associated with porphyroclastic relic of quartz, white mica I (1–0.5 mm), plagioclase, K-feldspar (Figure 7b). In this sample, biotite has been completely replaced by chlorite. Most quartz recrystallized showing small granoblastic grains while porphyroclastic plagioclase and K-feldspar are affected by brittle deformation.

[27] Sample 257, obtained from a white mica separate, exhibits a stair-case age spectrum. It increases from an initial age of ~112 Ma to a second step age of ~230 Ma, followed by generally increasing ages up to 273 Ma (Figure 9d).

[28] Within the Campo basement, in the immediate vicinity of the Eita shear zone, Permian and/or pre-Permian high-T fabrics are retrogressed and overprinted by a pervasive greenschist facies deformation. Two samples were taken for ^{40}Ar/^{39}Ar dating on white micas in the vicinity (<1 m) of the shear zone in the Campo unit. Analytical techniques and the ^{40}Ar/^{39}Ar stepwise heating results are provided in the auxiliary material and sample locations in Figures 4 and 5 and the auxiliary material.

[29] Sample 233 was collected from a deformed pegmatite dyke, presumably of Permian age, within the Campo basement at the immediate contact to the overlying Grosina unit (Figure 4). A relict magmatic assemblage consisting of quartz + K-feldspar + plagioclase + white mica I is largely overprinted by a greenschist facies fabric characterized by chlorite + clinozoisite + white mica II + quartz (Figure 7c). Porphyroclastic (<100 μm) white micas have been fractured and kinked while grain boundaries of porphyroclastic quartz show the formation of isolated small grains suggesting a bulging recrystallization processes (Figure 7c).

[30] Sample 233 shows a stair-case age spectrum, with an increase from an initial step of 100 Ma to ages of ~200 Ma at step 7 with 22% of the total ^{39}Ar released (Figure 9d). The majority of gas was released between steps 7–20 (78% of the total ^{39}Ar released) yielding apparent ages in the 200–210 Ma range (Figure 9d).

[31] Sample 17 was taken from a granitoid dyke displaying a pegmatitic texture in the vicinity of the Sondalo Gabbro affected by a greenschist facies overprint (Figure 4). The mineral assemblage consists of quartz + white mica + biotite locally weakly retrogressed to chlorite (Figure 7d). Quartz grains are highly strained and display undulose and patchy extinction, as well as deformation lamellae (Figure 7d). Newly crystallized fine-grained quartz crystals are observed along sutured poryphroclast boundaries, suggesting bulging recrystallization process (Figure 7d). Microstructures of quartz indicate temperature of deformation at approximately 300°C [e.g., *Stipp et al.*, 2002]. Porphyroclastic white micas show evidence of brittle deformation, including parting along basal cleavage and kinking (Figure 7d). Micas are elongated parallel to the foliation and are locally associated with fine-grained aggregates (Figure 7d).

[32] Sample 17 yields a relatively flat age spectrum, with the majority of the steps in the 201–205 Ma range (Figure 9c). The beginning of the age spectrum, starting from step 2, shows a slightly discordant shape between a minimum age of 197 Ma and a maximum age of 205 Ma (Figure 9c). Although two generations of white mica are found in the sample, the rare fine-grained aggregates of white mica have largely been selected out by hand picking. Therefore, the apparent age spectrum is interpreted as resulting from the degassing of the argon reservoir related to the large porphyroclastic white mica crystals.

6. Pre-Alpine Rift Related Structures in the Bernina Unit

6.1. Pre-Rift Structures and Their Relations to Mesozoic Sediments

[33] The Bernina unit is located next to the Campo-Grosina units in the footwall of the late Cretaceous Campo thrust fault. The restoration of *Mohn et al.* [2011] proposes that this thrust reactivated the pre-existing Grosina detachment, suggesting that these units were already juxtaposed in pre-Alpine time. The basement rocks of the Bernina unit are made of Carboniferous to early Permian (356–283 Ma) calc-alkaline and alkaline igneous rocks (Figure 4) intrusive into poly metamorphic Variscan basement associated with extrusive rhyolites and lamprophyric dykes [*Spillmann and Büchi*, 1993; *von Quadt et al.*, 1994]. Mesozoic sediments occur only locally as slices in the Piz Alv-Val da Fain, Val del Monte and Sassalb areas (Figure. 4). At Piz Alv (Figures 4, 5, and 10), a complete pre-rift succession is preserved including Permian rhyolites, massive shallow marine Triassic dolomites and Upper Triassic lagoonal sediments, overlain by Lower Jurassic limestone. The whole sequence is 600 to 800 m thick and shows, except for the Lower Jurassic limestone, a very similar evolution to that observed in the more proximal parts of the Adriatic margin (e.g., Ortler and Ela units). The age of the lower Jurassic limestone (Agnelli Formation (Fm.)), representing the last pre-rift formation, has been constrained by ammonites indicating a Sinemurian age for the deposition and an early Pliensbachian age (188 Ma) for the hardground at the top of this formation [*Finger*, 1978; *Manatschal and Nievergelt*, 1997]. Syn-rift sedimentation began with the deposition of 200 to 300 m thick breccias, referred to as the Alv Breccia [*Schüpbach*, 1974] in Piz Alv (Figure 10a). These breccias consist exclusively of clasts of Triassic and Lower Jurassic carbonate that range in size from some few mm to several tens of meters. Previous authors [*Schüpbach*, 1974; *Furrer et al.*, 1985; *Froitzheim*, 1988] interpreted these breccias as formed in situ or by minor gravitational transport on the flanks of submarine highs related to high-angle fault activity

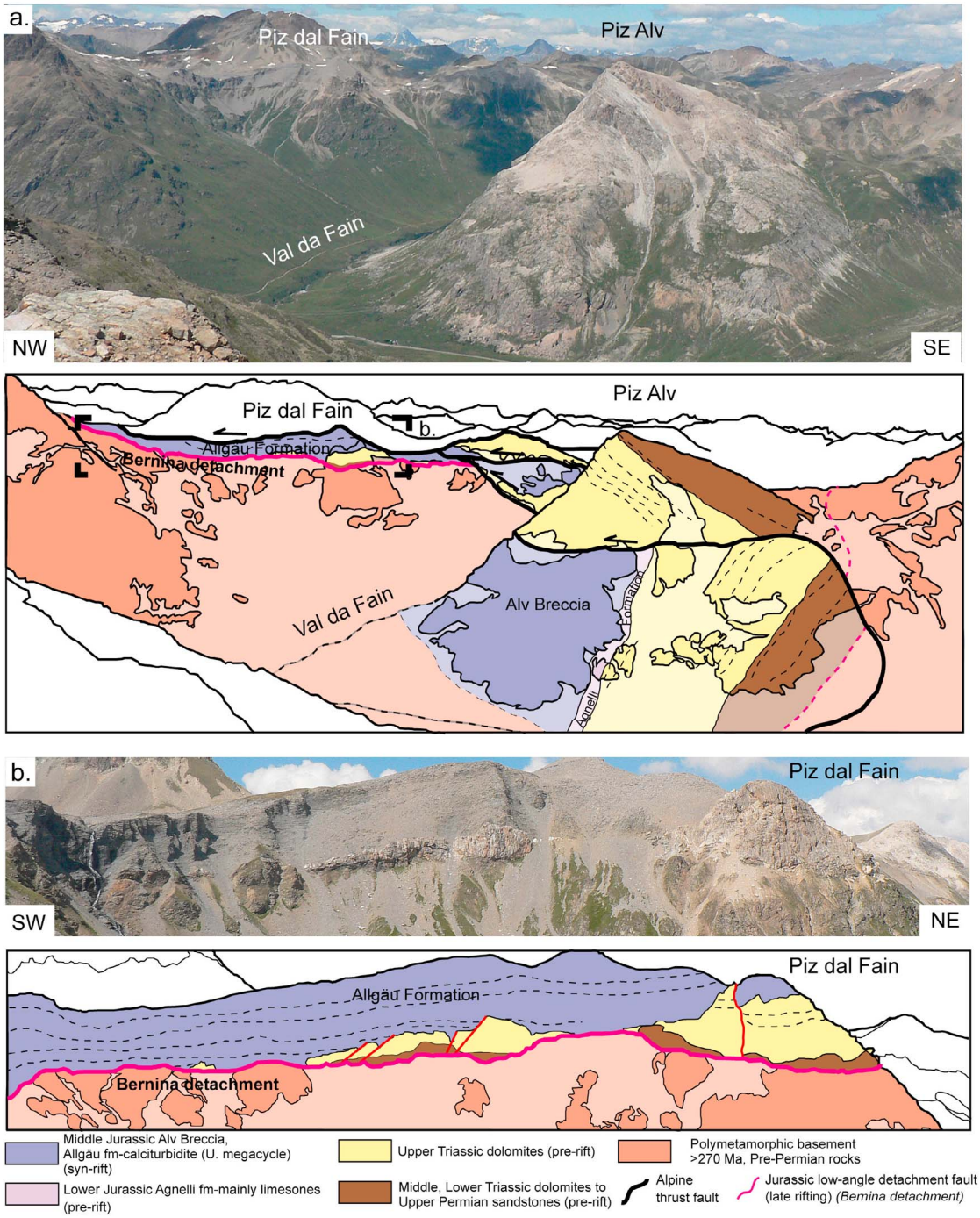

Figure 10. Photograph and line drawing from the Piz Alv–Val dal Fain area (Bernina unit) (for location of the photograph see Figures 4 and 5a). (a) Large-scale structure of Piz Alv-Val da Fain area viewed from the S showing the relationship between pre- and syn-rift sediments and basement rocks (796000/148000) (for restoration see Figure 5c). (b) View of Piz dal Fain from the S showing the syn-rift sediments (Allgäu Fm. (upper mega-cycle)) onlapping either onto exhumed basement or pre-rift sediments. (795000/149000) (for more details see text). Coordinates are given with the Swiss grid.

during the rifting. Laterally, the Alv breccias pass into calciturbidites, marls and hemipelagic limestones, dated as Late Sinemurian to Bathonian and referred to as the Allgäu Formation (Fm.) [*Eberli*, 1988]. The overall sequence shows a general thinning- and fining upward megacycle interpreted to represent a basinal sequence ranging in thickness between 200 and 500 m that was deposited in fault-bounded rift basins [*Eberli*, 1988]. To the northwest at Piz dal Fain (Figures 4, 5, and 10), the syn-rift Allgäu Fm. directly overlies and seals Paleozoic basement and discontinuous and dismembered slices of pre-rift sediments (Figure 11b). The Allgaü Fm. is onlapping at a low angle (<20°) onto

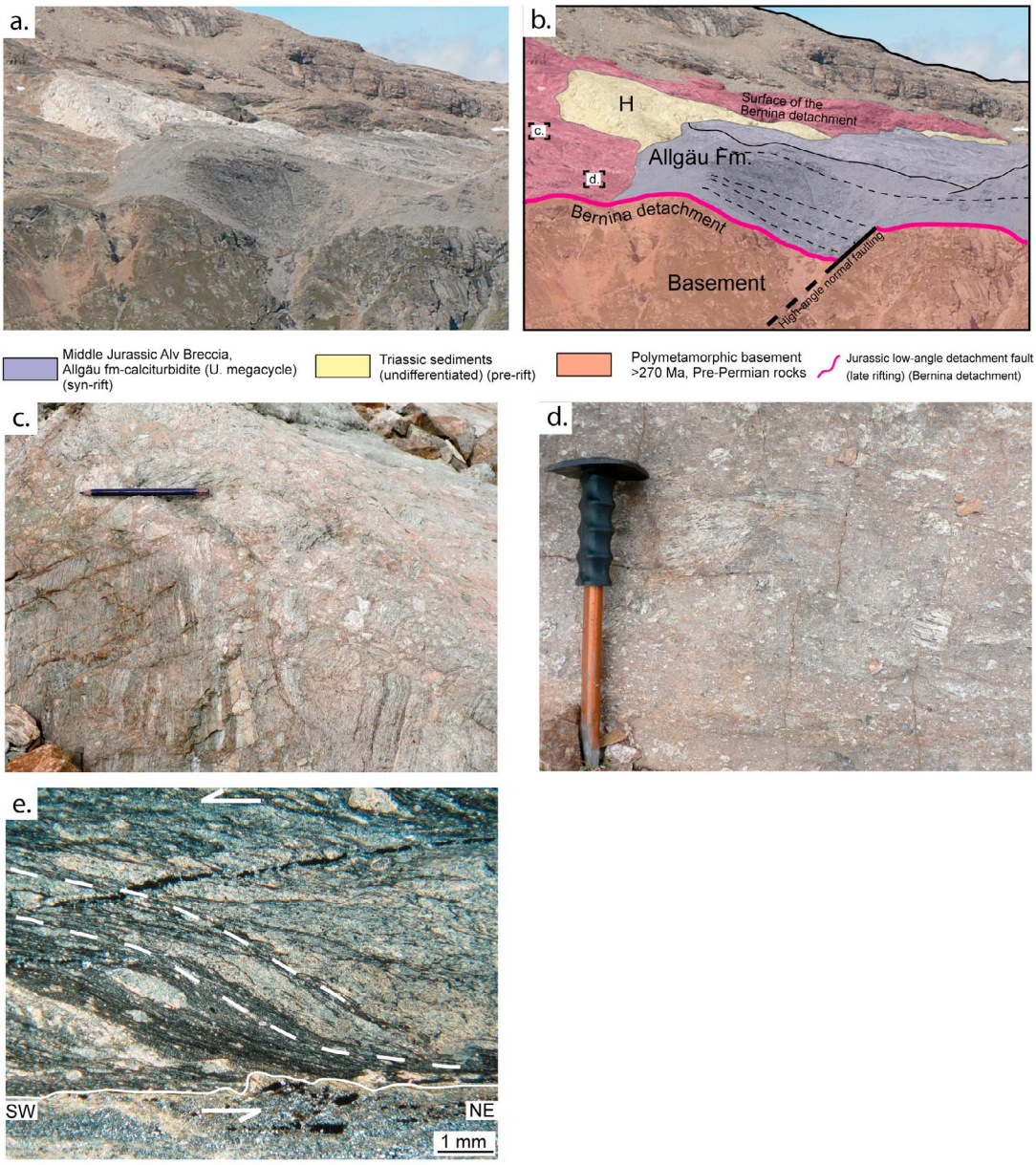

Figure 11. (a) Photograph and (b) line drawing of the Bernina detachment (Bernina unit) (view from the south). High-angle normal faults crosscutting the Bernina detachment can be locally observed. The syn-rift Allgäu Fm. thickens toward this fault, indicating that these sediments were deposited during the activity of this structure (794983/149072). View of the fault rocks related to the Bernina detachment. (c and d) Cataclastically deformed Paleozoic basement of the Bernina unit (794832/149133). (e) Photomicrographs under crossed polarizers of a gouge layer showing rotation of the shear fabric during shearing indicating a top to SW sense of shear (794643/143200). Coordinates are given with the Swiss grid. For location of the photographs see Figure 4 and 5.

Paleozoic basement or pre-rift slices. *Schüpbach* [1974] interpreted the relation between the pre-rift slices and the syn-rift Allgäu Fm. as strictly sedimentary. These slices, overlying the basement, show a variable and reduced pre-rift sedimentary cover ranging from several tens to a few meters thick. This situation is very different from the thick (~800 m) and constant pre-rift cover record on the whole Austroalpine unit and in Piz Alv (Figure 10a). These slices are generally made up of Upper Triassic dolomites associated with a reduced middle to lower Triassic and Permian succession (Figure 10b). These slices are strongly dismembered by small-scale (~m) high-angle normal faults, which cannot be observed in the surrounding basement or syn-rift sediments.

6.2. Bernina Detachment

[34] The Bernina detachment represents a major structure that can be mapped over more than 20 km, separating Paleozoic basement rocks in the footwall from basement blocks associated with Permian rhyolites, pre-rift and syn-rift sediments in the hanging wall (Figures 4 and 5).

Although this fault is in most places reactivated by subsequent Alpine thrust faults, the pre-Alpine architecture is locally preserved. In Val dal Fain, the detachment is characterized by a 1 to 20 m thick damage zone of brittle fault rocks located at the top of the basement (Figures 11a–11d). Mylonites or other evidence for deformation at deeper crustal levels are not observed associated with this brittle detachment. Locally, matrix-supported fault gouges with rounded, footwall-derived clasts can be observed (Figure 11e). They are best developed where the top of the basement is overlain by Permian rhyolites. Stretching lineations are oriented in a NE-SW direction and, based on shear bands and asymmetric strain fringes around porphyroclasts of K-feldspar, a top to the southwest sense of shear can be determined (Figures 4 and 11e).

[35] At Piz Alv, the Bernina detachment can be mapped at the interface between Paleozoic basement and a complete pre-rift succession (Figures 4, 5, and 10a). Therefore we interpret Piz Alv as an extensional allochthon (Figures 5c). On the northern side of Val dal Fain, the fault surface is in turn overlain by extensional allochthons consisting of upper crust and pre-rift sediments or onlapped at a low angle (<20°) by the syn-rift Allgäu Fm. (Figures 5c and 10). The top of the fault is formed by a smooth surface with local fissures filled by indurated tectono-sedimentary breccias. Pre-rift slices on top of Bernina detachment are crosscut by small scale high-angle normal faults, which are sealed by syn-rift sediments (Figure 10b). This complex geometry implies that the pre-rift succession was emplaced tectonically onto the basement and does not represent olistolites. This indicates that the top basement surface formed as a tectonic surface that was locally exposed at the seafloor. Similar top basement detachment faults have been described also from the Err unit [e.g., *Manatschal and Nievergelt*, 1997; *Masini et al.*, 2011]. Where the detachment surface is onlapped by the Allgäu Fm., no gouges are observed and basement clasts do not occur in the overlying sediments. This suggests that exhumation was followed by erosion and removal of the gouges and cataclastic basement, before the basement was sealed and onlapped by the Allgäu Fm. Although in the direct neighborhood basement-derived breccias are not observed, they occur in the adjacent Err unit, located more oceanward, in the Middle Jurassic Saluver Fm. (Figure 3).

[36] The age of Bernina detachment can be inferred from high-angle faults with vertical displacements ranging from 10 to 600 m cutting the Bernina detachment (Figures 11a and 11b). Because the basal sediments thicken toward these high-angle faults, and higher levels of the same formation sealed these faults, it had to form during the sedimentation of the Allgäu Fm. Thus, the basal sediments of the Allgäu Fm. were deposited during or after exhumation of basement along the Bernina detachment fault, but before the end of tectonic activity in this domain. These relationships confirm the Jurassic age of the Bernina detachment.

7. Discussion

[37] Understanding of the processes and mechanisms associated with extreme crustal thinning requires direct access to tectonic structures and rocks from the necking zone of rifted margins. Based on the new observations and data of the Campo-Grosina and Bernina units presented above and on existing data from the Adriatic rifted margin, in this section we discuss the structures, processes and the timing related to crustal thinning within the Alpine Tethys rift system. This will allow us to propose a new coherent conceptual model to explain extreme lithospheric extension and to evaluate its implications for the interpretation of present-day rifted margins.

7.1. Structures Related to Crustal Thinning: The Eita Shear Zone

[38] In the Valle Grosina, the contact between Campo and Grosina basements is characterized by the presence of the Eita shear zone. Previous studies [*Meier*, 2003] suggested that this shear zone was formed during late-Cretaceous thrusting. However, stretching lineations along this structure indicate a NNW sense of shear, which is oblique with respect to the generally NW-SE direction of transport along Alpine and Jurassic rift-related structures in the area [*Froitzheim and Manatschal*, 1996]. This observation indicates an oblique component for motion along the shear zone with respect to other rift structures, provided that the study area did not experience regional-scale rotation during the Alpine orogeny. As discussed below, the $^{40}Ar/^{39}Ar$ geochronological data presented in this study provides clear indication that a significant amount of crustal excision was accommodated along the Eita shear zone in the Late Triassic-Lower Jurassic. Local Alpine reactivation of this structure is possible and indeed likely. However, as discussed below, the regional cooling pattern indicates that its activity was largely restricted to the Late Triassic-Lower Jurassic.

[39] White mica and biotite separated from the Campo basement in the footwall of the Eita shear zone consistently yield ages ≤205 Ma (Figures 9 and 12). Biotite separated from samples 6 and 32 belonged to a high-T metamorphic fabric that was generated during emplacement of the Sondalo Gabbro at middle to lower crustal depth at ca. 270–300 Ma. These biotites yield ages in the 183–189 Ma range (Figures 9a, 9b, and 12). Sample 32 yielded the most concordant spectrum. This sample is characterized by a pervasive high-T metamorphic fabric with only one generation of biotite (Figure 7e), which yielded a relatively flat age spectrum in the 179–185 Ma range (Figure 9a). This estimate is more than 85 Myr younger that the inferred Permian age of the metamorphic fabric. The complete lack of chloritization of the biotites visible under the optical microscope allows to rule out this process as a possible cause of argon loss [*Di Vincenzo et al.*, 2003]. Therefore, the Jurassic ages of the spectrum are interpreted as being related to cooling of the studied biotites below a temperature of ca. 300°C during the exhumation from middle/lower crustal depth (closure T is estimated from *Harrison et al.* [1985], for the cooling rate of 10°C/Ma estimated by *Braga et al.* [2001] for the plutonic rock of the Sondalo area). Sample 6 yields similar results, although with a slightly more discordant age spectrum, which may be related to the fact that the rock sample contained 3 generations of biotite with different grain sizes and, likely, slightly different Ar retention (Figure 9b).

[40] White mica from samples 17 and 233, which also belong to the Campo basement, yielded slightly older ages than biotite (Figures 9c and 9d). Both samples were taken

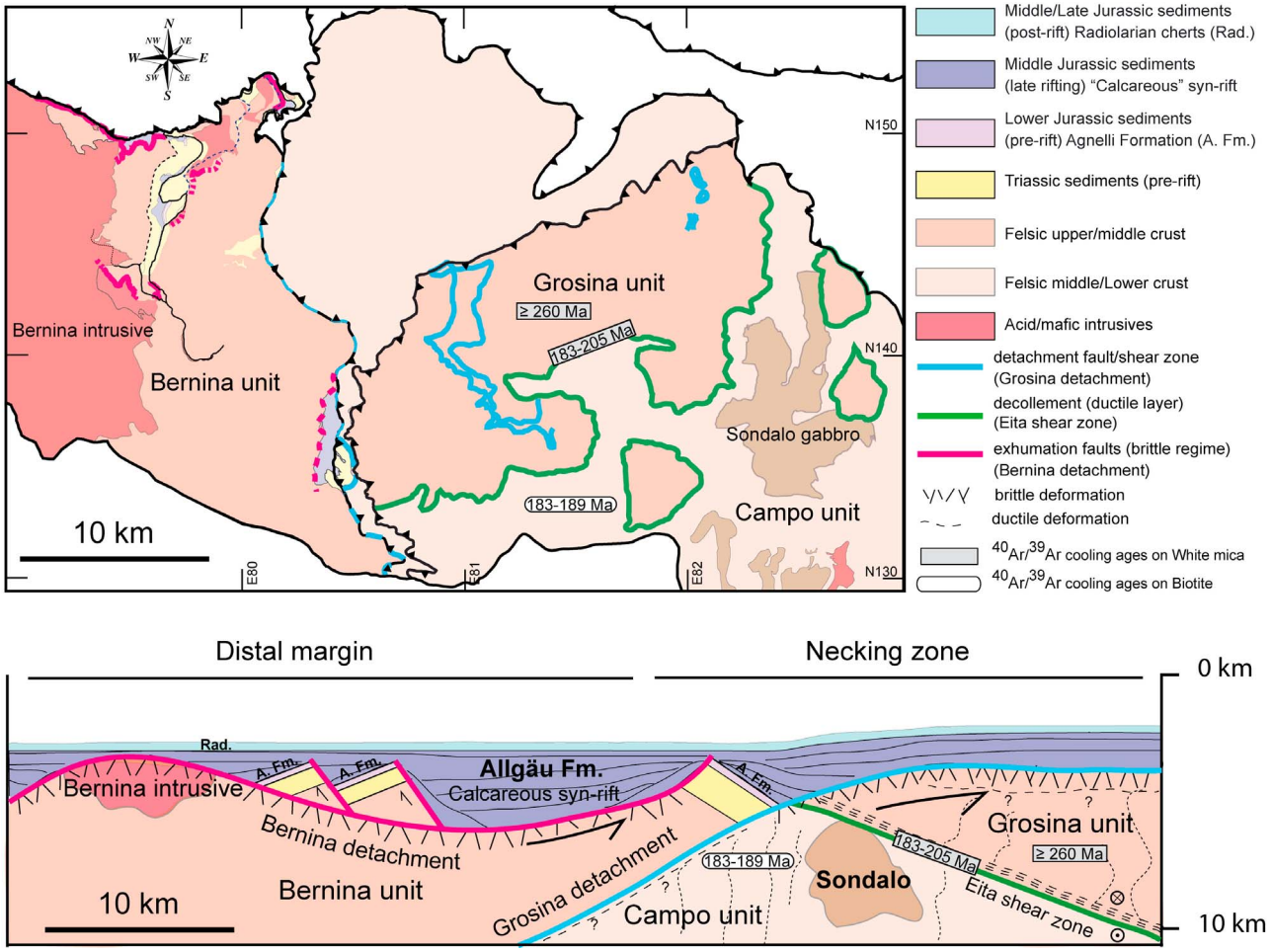

Figure 12. Present-day geological map associated with a restored cross-section of the necking zone of the Adriatic rifted margin across the Bernina-Campo-Grosina units. The cross section summarizes the sediment architecture, fault geometry, $^{40}Ar/^{39}Ar$ data, and strain distribution observed in these units.

from the upper part of the Campo basement, less than 10 m from the contact with the Grosina basement. Sample 17 yielded a relatively flat age spectrum, with the majority of steps, between steps 8–13 (68% of the total ^{39}Ar released) in the 201–205 Ma range (Figure 9c). The age spectrum of sample 233 is characterized by a progressive age increase, with the majority of apparent ages (steps 7 to 17) falling in the 198–207 Ma range (Figure 9d). Although two generations of white mica are found in the studied samples, the rare fine grained aggregates (<100 μm) of white mica defining the mylonitic fabric of the Eita shear zone have largely been selected out by hand picking. Therefore, the apparent age spectrum of both samples is interpreted as resulting from the degassing of the argon reservoir related to the large porphyroclastic white mica crystals. The measured ages are likely to record cooling of the porphyroclastic white micas below temperatures at which a significant amount of radiogenic argon could be retained in the crystal lattice. This interpretation is supported by the $^{40}Ar/^{39}Ar$ age of 188 ± 4 Ma obtained by *Meier* [2003] from white micas of the Campo basement. The Cretaceous ages obtained in the first 2 steps of the heating experiment from samples 208, 257, 233 may hint at local re-setting/recrystallization during the Alpine orogeny (Figure 9d).

[41] $^{40}Ar/^{39}Ar$ ages of white micas from the Grosina basement are significantly older than those found in the Campo basement (Figure 9). As discussed above, the base of the Grosina basement is overprinted for a thickness of about 200 m by a pervasive greenschist facies flat-lying fabric related to the Eita shear zone (Figures 4 and 6e). Samples 208, 257 were located within this overprinted area, respectively at 100 m and in the vicinity (~1 m) of the contact with Campo basement (Figures 4, 7a, 7b, and 9d). Both samples yielded staircase $^{40}Ar/^{39}Ar$ age spectra. Similarly to the Campo basement, samples 208 and 257 contained two generations of white micas (Figures 7a and 7b). Also in this case, the finest grained white mica II was selected out by hand picking. Therefore, the age spectra are interpreted to be derived largely from degassing of the coarse-grained porphyroclastic white mica I. Sample 208, which was located further away from the contact with the Campo basement and is less affected by the greenschist facies shear fabric yield Permian ages in the 250–275 Ma range over 86% of the radiogenic argon release (Figure 9d). Sample 257, instead, yielded slightly younger ages, with Triassic ages over 50% of the radiogenic argon release (Figure 9d).

[42] Shifting of the age spectrum toward younger ages from sample 208 to sample 257 is probably a result of the

more pervasive overprint during shearing along the Eita Shear Zone (Figure 9d). Therefore, the $^{40}Ar/^{39}Ar$ geochronology performed on the Grosina basement indicates that the analyzed porphyroclastic white micas cooled in the Permian and were later partly reset during the activity of the Eita shear zone.

[43] The very fine-grained micas that define the mylonitic fabric of the Eita shear zone have not been dated in this study. Despite this, an Upper Triassic-Lower Jurassic age can be proposed for the activity of the Eita Shear Zone on the following grounds:

(1) The Eita shear zone juxtaposes rocks with Permian or older white mica cooling ages (>260 Ma) in hanging wall (Grosina basement) against rocks with younger cooling ages (~205–183 Ma) in the footwall (Campo basement; Figure 12). This age gap brackets the time of activity of the interface between the Campo and Grosina units;

(2) Flat age spectra of biotites from the Campo basement (samples 6 and 32), which did not experience any fabric reworking after the Permian, allows us to exclude any argon loss during the Alpine orogeny. Such argon loss would have been inevitable if the Grosina basement had been thrust over the Campo basement in Alpine times at the conditions of 350–400°C estimated from the metamorphic and microstructures observed along the Eita shear zone.

(3) An Alpine activity is inconsistent with the observed structural style as well as the Alpine kinematics. Indeed, in the study area, Alpine thrust faults are constantly described as narrow shear zones (~m) with synkinematic metamorphic conditions around 300°C [e.g., *Froitzheim et al.*, 1994; *Ferreiro Mählmann*, 1996]. Furthermore the main thrusting event shows a dominance of WNW-shear sense. These characteristics are significantly different from those displayed by the Eita shear zone. Nevertheless, local Alpine reactivation of this structure as inferred by *Meier* [2003] is considered to be likely, and is compatible with Late Cretaceous ages obtained in the earliest steps of the step-heating experiments in samples 208, 257, 233. However, such low-grade Alpine reactivation would have resulted in minor reworking of an already established large-scale crustal section (for details see *Mohn et al.* [2011]).

[44] Furthermore, the substantial gap in $^{40}Ar/^{39}Ar$ ages between the Campo and Grosina units indicates that while the Grosina basement was already residing in an upper to mid-crustal position (T < 400°C) in the Permian, the Campo basement was still at temperatures sufficient to cause significant argon diffusion in white mica (~405°C for a grain with a 100 μm radius cooling at 10°C/km and ca. 5 kbar [*Harrison et al.*, 2009]). This conclusion is also supported by the intrusion of the Sondalo Gabbro at a mid- to lower crustal position (0.6 ± 0.2 GPa) [*Tribuzio et al.*, 1999; *Braga et al.*, 2001, 2003], which constrains the Permian depth of the Campo basement to ca. 15–25 km. Therefore, the Eita shear zone marks a significant crustal gap, indicating that it must have been active as an extensional shear zone (Figure 12). Based on the metamorphic conditions and microstructures it can be proposed that the Eita shear zone was active between 400 and 300°C. Assuming a thermal gradient of ca. 20–25°C/km as inferred for the Triassic time by *Müntener et al.* [2000], this would indicate that this structure was active at 10 to 15 km depth separating pre-rift middle/lower crust (Campo basement) from pre-rift upper/middle crust (Grosina basement). Since this structure can be mapped along 20 km juxtaposing the same crustal levels and showing the same metamorphic conditions, we propose that this shear zone was active as a decollement horizon between a ductile upper/middle crust (Grosina) and rigid "brittle" middle/lower crust (Campo) (Figure 12). Several similar shear zones have been identified in the Campo and Grosina units. Although their exact role and age are not yet determined, we do not exclude that these shear zones may belong, together with the Eita shear zone, to a network of shear zones responsible for thinning of the ductile middle crust during rifting.

7.2. Structures Related to Exhumation: The Grosina Detachment

[45] The type locality of the Grosina detachment is located at Sasso Campana, where this low-angle intrabasement detachment fault is exposed at the top of the Grosina basement (Figures 4, 5b, 5c, and 8). We suggest that this structure can be correlated with the pre-Alpine brittle fault observed in the Sassalb area located more to the west, where it separates the exhumed mid- to lower crustal rocks of the Campo basement from pre-rift Triassic dolomites and upper crustal rocks of the Bernina unit (Figures 8a and 8b). Thus, in the Sassalb area, the Grosina detachment marks the contact between the Grosina-Campo units in the footwall and the Bernina unit in the hanging wall (Figures 8a and 8b). Crosscutting relationships allow the age of this structure to be constrained. At Sassalb, the Grosina detachment is folded and truncated by Alpine Campo and Grosina thrust faults, indicating that it pre-dates Late Cretaceous Alpine convergence (Figure 5). The observation that along this detachment Permian middle/lower crustal rocks (Campo basement) are juxtaposed against Triassic dolomites (Bernina unit) excludes a Permian or older age. This is also in line with the observation that the Grosina detachment cuts across Permian high-T fabrics in the Grosina and Campo units. Therefore a Jurassic age can be proposed for the Grosina detachment. From a map view, this interpretation seems to be confirmed by the fact that Grosina detachment crosscuts the Late-Triassic to Early Jurassic Eita shear zone (Figure 5). In contrast to the latter, we interpret the Grosina detachment as a downward concave exhumation fault along which rocks from deeper crustal levels, i.e., Grosina and Campo units, were exhumed and juxtaposed against upper crustal rocks and Mesozoic sediments, i.e., Bernina unit (Figure 12). Structural and microstructural observations show that the Grosina detachment fault was active in the brittle field below ~300°C probably during Jurassic rifting. Significantly, within this brittle detachment, clasts of higher grade mylonitic rocks can be found, indicating brittle reworking of pre-existing ductile shear fabrics (Figures 8e and 8f). Crosscutting relationships between the brittle Grosina detachment and these quartz mylonites indicate an angular discordance of about 20°. Three main possibilities can be proposed to account for the mutual relationship between quartz mylonites and detachment: (1) the quartz mylonites formed in a deeper part of the Grosina detachment and were exhumed and overprinted by brittle deformation, or (2) the quartz mylonites belong to a structure similar to the Eita shear zone, i.e., they represent a decollement that was exhumed along the detachment fault (e.g., mylonitic

front along the Wipple Mountains detachment [*Lister and Davis*, 1989]), or (3) the quartz mylonites are unrelated to Jurassic rifting and were formed as a result of Permian or Variscan tectonics. At the moment the exact significance of this quartz mylonite remains unclear.

7.3. A Low-Angle Top Basement Detachment Fault in the Distal Margin: The Bernina Detachment

[46] The Bernina detachment is interpreted as a low-angle top basement detachment fault accommodating the final extension in the distal margin (Figure 12). In the Val dal Fain and Piz Alv area (Figure 10), the first phase of rifting is characterized by high-angle normal faulting associated with the deposition of the Alv breccias. The high-angle normal faults of this earlier rift phase have been subsequently crosscut by younger low-angle detachment faults. This results in the formation of extensional allochthons that range in scale from several tens of kilometer wide blocks (e.g., Piz Alv), including basement, to small, extended fragments of pre-rift dolomites overlying exhumed basement (e.g., Val dal Fain; Figure 10b). Along the Bernina detachment, no variation of the metamorphic conditions can be observed and the structures related to the detachment are forming in the brittle field at temperatures below 300°C over more than 20 km in the direction of transport (Figures 4 and 11). This observation suggests that this fault was only active in the brittle field within the upper crust. Although it is difficult to determine the initial dip of the fault at depth, near the surface the fault was sub-horizontal and was exhumed at the seafloor, resulting in a low-angle top basement detachment fault. This is confirmed by the low-angle between the fault zone and the syn-rift sediments onlapping onto the fault (Figure 10b). The lower limit for the activity of the Bernina detachment can be inferred from truncation of the youngest pre-rift formation dated as Pliensbachian [*Finger*, 1978], while the last part of the Allgäu Fm., which was deposited in a post-tectonic setting until the Bathonian, provides the upper limit [*Furrer et al.*, 1985, *Eberli*, 1988]. The Bernina detachment is interpreted as a similar structure to the Err detachment [*Froitzheim and Eberli*, 1990; *Manatschal and Nievergelt*, 1997; *Manatschal*, 1999, *Masini et al.*, 2011], but located in a part of the distal margin closer to the continent (Figure 3). These structures accommodated extension in the distal continental margin, similar to the structures described from the present-day Iberia distal margin, which are responsible for mantle exhumation.

7.4. The Temporal and Spatial Evolution of Crustal Thinning (Figure 13)

[47] To unravel the temporal and spatial evolution of crustal thinning along the fossil Adriatic rifted margin, several data sets need to be taken into account and correlated: (1) the stratigraphic record, (2) petrological and thermochronological data obtained from the basement units, and (3) the structures accommodating crustal thinning. While the stratigraphic record can be deduced from the whole margin system, including the conjugate European/Briançonnais margins (for a review see *Mohn et al.* [2010]), the exhumation and thinning in the basement can only be determined from locations where the Alpine tectonic and metamorphic overprint allowed the preservation of rift structures.

7.4.1. Initial Condition at the Onset of Rifting and Importance of Inheritance (Figure 13a)

[48] The pre-rift setting of the future Adriatic and Briançonnais/European margins, i.e., the future conjugate margins, was characterized during the Triassic by widespread shallow marine carbonate platforms, which suggest that the pre-rift crust was thermally and isostatically equilibrated (Figure 13a). This is confirmed by petrological work from the crust-mantle section preserved in the Margna/Malenco domain (Braccia gabbro). *Müntener et al.* [2000] demonstrated that before rifting in Triassic time the base of the crust was located at ca. 25–30 km, at metamorphic conditions of T = 600 ± 50°C and P = 0.8 GPa, suggesting an average heat flow of 70 W/m^2 (Figure 13a).

7.4.2. From Stretching to Thinning: Birth of the Necking Zone (Figures 13b and 13c)

[49] The first extensional structures related to Jurassic rifting initiated during Late Triassic to Late Sinemurian time (~205–190 Ma) (Figure 13b). These structures form large basins bounded by high-angle normal faults (e.g., Ortler unit; [*Eberli* 1988]). In the Southern Alps, *Bertotti* [1991] recognized the listric geometry of Jurassic normal faults and demonstrated that these faults sole out under greenschist facies conditions at mid-crustal levels around 10–15 km (Figure 13). This suggests that, during early rifting, deformation in the upper crust was decoupled from deformation in the mafic lower crust and subcontinental mantle. Moreover, exhumation of basement rocks (upper crust) occurs only along fault scarps related to the listric normal faults bounding the early rift basins (Figure 13b). This, together with the overall subsidence of the margins, explains why no basement was yet exhumed and reworked in the stratigraphic succession of the Alpine Tethys margins during this early stage of rifting (Figure 13b). The same style of deformation is also observed on the European margin (e.g., Bourg d'Oisans [*Lemoine et al.*, 1986]). Attempts to quantify the extension accommodated in the upper crust results in β-factors ranging between 1.2 and 1.65 [*Froitzheim*, 1988; *Bertotti et al.*, 1993; *Chevalier et al.*, 2003].

[50] From Pliensbachian to Toarcian (190–175 Ma), extension starts to shift toward the future distal margin [*Froitzheim and Eberli*, 1990], resulting in a major change in the structural and stratigraphic evolution of the whole margin (Figure 13c). In the Bernina unit, this period is characterized by deposition of the Alv Breccia in fault-bounded basins linked with the deposition of the second megacycle of the Allgäu Fm. During Toarcian to Aalenian time (180–

Figure 13. Conceptual model showing the evolution of lithospheric thinning as recorded in the Adriatic fossil margin: (a) the pre-rift situation in middle Triassic, P-T condition during the Triassic time for the lower crust are inferred from the Braccia and Fedoz gabbros at 600 ± 50°C and 0.8 ± 0.1 GPa [*Müntener et al.*, 2000], (b) stretching phase from late Triassic to Sinemurian (220 to 190 Ma), (c) thinning phase from Pliensbachian to Toarcian (190 to 175 Ma), and (d) exhumation phase from Toarcian to Callovian (175 to 161 Ma). Note the spatial and temporal evolution of the Bernina intrusive, Sondalo and Braccia Gabbro.

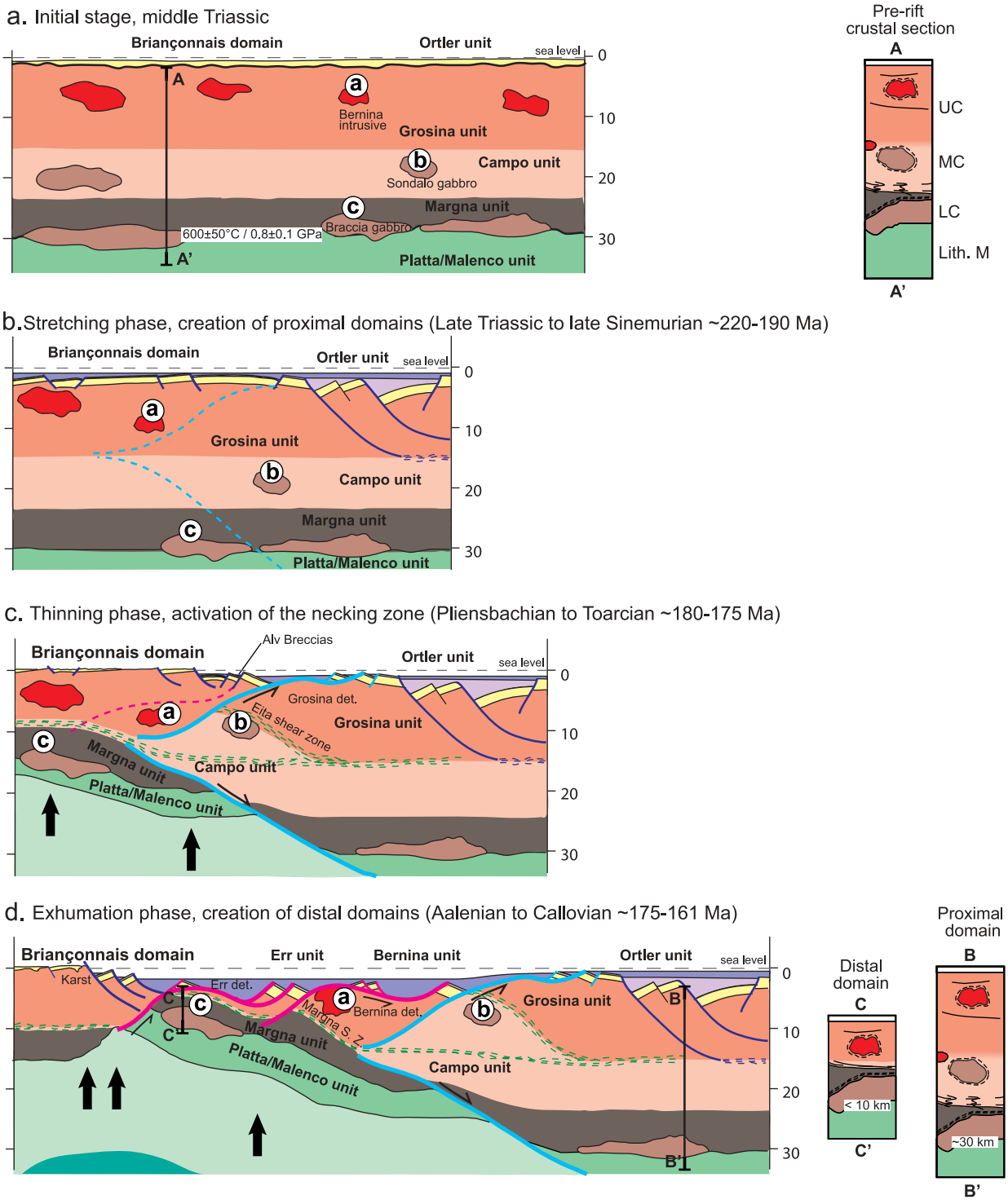
a. Initial stage, middle Triassic
Briançonnais domain
Ortler unit
sea level
Bernina intrusive
Grosina unit
Campo unit
Sondalo gabbro
Margna unit
Braccia gabbro
600±50°C / 0.8±0.1 GPa
Platta/Malenco unit
Pre-rift crustal section
UC
MC
LC
Lith. M
b. Stretching phase, creation of proximal domains (Late Triassic to late Sinemurian ~220-190 Ma)
c. Thinning phase, activation of the necking zone (Pliensbachian to Toarcian ~180-175 Ma)
Alv Breccias
Grosina det.
Eita shear zone
d. Exhumation phase, creation of distal domains (Aalenian to Callovian ~175-161 Ma)
Err unit
Bernina unit
Karst
Err det.
Bernina det.
Margna S.Z.
Distal domain
Proximal domain
< 10 km
~30 km
Middle Jurassic sediments (late rifting) "Calcareous" synrift (Allgäu Fm-upper megacycle)
Lower Jurassic sediments (early rifting) (Allgäu Fm-lower megacycle in Ortler unit-syn-rift/ Agnelli Fm. in Err, Bernina unit-pre-rift))
Triassic sediments
Upper/middle crust
Middle crust
Lower crust
Acid and mafic intrusives
Subcontinental mantle
Infiltrated subcontinental mantle
Asthenospheric mantle
successively younger faulting systems
Exhumation faults
Detachement faults
Decollements
Stretching faults
Future faults
Ductile decoupling

Figure 13

170 Ma), the Briançonnais domain undergoes a different and decoupled evolution from the rest of the margin. This is indicated by an uplift leading to subaerial exposure, indicated by the occurrence of karst and subaerial sediments, which is in contrast to the subsidence recorded on the adjacent proximal margins (Figure 13c). The subaerial conditions prevailed until the Bathonian-Oxfordian (165–155 Ma), when the Briançonnais domain subsided rapidly.

[51] Significantly, this distinctive changes in palaeobathymetry occurred at the same time as crustal thinning within the continental crust in (1) the Ivrea-Verbano zone in the Southern Alps (Figure 2 section B-B′) and (2) in the Grosina-Campo units in the Eastern Alps (Figure 2 section C-C′). The new Grosina-Campo data provide critical constraint on the shallow part of the necking zone, whereas the Ivrea-Verbano zone preserves the deeper parts of the necking zone, which are not exposed in the Campo-Grosina units. In these units, new $^{40}Ar/^{39}Ar$ data on biotite from the Campo basement, sampled in the vicinity of a Permian intrusion (Sondalo Gabbro) (Figure 13c) demonstrate that these rocks were exhumed and cooled below ca. 300–350°C at around 200–180 Ma. A similar evolution has been proposed for the Ivrea-Verbano Zone, which was intruded by Permian gabbros in a lower crustal position (∼30 km) [*Handy et al.*, 1999; *Mulch et al.*, 2002, and references therein]. In this zone, pre-rift upper/middle crust (e.g., Strona-Ceneri) was juxtaposed against lower crustal levels (e.g., Ivrea-Verbano zone) along the Pogallo shear zone (Figure 2; section B-B′) [e.g., *Handy*, 1987; *Handy et al.*, 1999]. P-T-t paths from the Ivrea-Verbano zone indicate that pre-rift lower crust was exhumed below temperatures of 350–320°C at ca. 170–220 Ma [*Mulch et al.*, 2002]. Therefore, previous studies interpreted the Pogallo shear zone as an extensional moderate- to low-angle detachment fault (10 to 34°) along which the Ivrea-Verbano lower crustal rocks were exhumed to a depth of 10 km during Jurassic rifting [e.g., *Handy*, 1987; *Mulch et al.*, 2002; *Handy and Zingg*, 1991]. Exhumation of deeper levels of the continental crust was contemporaneous with uplift of the Briançonnais domain. The observation that crustal attenuation occurred simultaneously with the uplift of the Briançonnais domain is a key observation at odds with the classical model of *McKenzie* [1978]. However, such anomalous subsidence histories are commonly observed in hyper-extended rifted margins (e.g., Iberia margin [*Péron-Pinvidic and Manatschal*, 2009]; South Atlantic and NW-Australia margin; [*Driscoll and Karner*, 1998]). It can be best explained if crustal thinning occurred simultaneously with thinning of the mantle lithosphere. In the case of the Alpine Tethys system, *Piccardo* [2008] and *Müntener et al.* [2010, and references therein] showed that lithospheric thinning was related to the impregnation of magma into subcontinental mantle prior to its exhumation at the seafloor. The magma-infiltration may have enhanced the thermal erosion, resulting in depth-dependent thinning of the lithosphere [e.g., *Kusznir and Karner*, 2007; *Cannat et al.*, 2009].

7.4.3. From Thinning to Exhumation (Figure 13d)

[52] Final rifting is characterized by the localization of deformation in the future distal margin over previously thinned crust (Figure 13d). A relic of a crustal section across the Adriatic margin prior to exhumation is preserved in the Margna unit in the eastern Alps (Figure 2, section C-C′). In this area, pre-rift lower crustal rocks preserving a primary contact with subcontinental mantle welded by a Permian gabbro (Braccia gabbro) are juxtaposted against pre-rift upper crust preserving primary contacts with Mesozoic sediments through the activity of an extensional shear zone (e.g., Margna shear zone in section C-C′ [e.g., *Guntli and Liniger*, 1989; *Hermann and Müntener*, 1996; *Hermann et al.*, 1997; *Bissig and Hermann*, 1999]). This shear zone is located at the interface between uppermost and lowermost crust with more than 25 km of continental middle crust missing in-between [e.g., *Hermann and Müntener*, 1996; *Bissig and Hermann*, 1999]. We suggest that horizontal extension of the continental crust was achieved with the extreme thinning of ductile quartzo-feldspatic mid-crustal levels. At this stage, the new faults cut through an already thinned, brittle crust and are able to penetrate into the underlying subcontinental mantle. These new structures form low-angle top-basement detachment faults that result in the delamination of the hanging wall and the exhumation of upper crust and eventually also lower crust, leading finally to exhumation of subcontinental mantle at the seafloor (Figure 13d). The top-to-the-west (ocean) sense of shear determined from these detachment faults is in line with these faults forming breakaways to the east (continent) that cut westward (oceanward) into the mantle. The allochthons occurring over the detachment faults (e.g., Val dal Fain–Piz Alv area; Figures 5a and 10), are interpreted to derive from the delamination of the hanging wall block, i.e., the Briançonnais domain. This interpretation is supported by the similarity between the pre-rift stratigraphic record of the Briançonnais and the distal Adriatic margins.

[53] The formation of exhumation surfaces is best recorded in the stratigraphic record by the occurrence of reworked crustal rocks in the syn-rift sediments, suggesting the creation of a new siliciclastic sediment source [*Masini et al.*, 2011]. In the Southern Alps, in the Canavese zone (Figure 2, section B-B′), the exhumation of lower crustal rocks is indicated by the occurrence of clasts derived from the lower crust in the syn-rift sediments [*Ferrando et al.*, 2004]. Finally, low-angle top-basement detachment faults permit the exhumation of subcontinental mantle to the seafloor (Figure 13d). A maximum age for this exhumation is given by the 165 to 160 Ma U/Pb ages on zircons from oceanic gabbros that have been exhumed to the seafloor and a minimum age is given by the age of the radiolarian cherts stratigraphically overlying the exhumed mantle, which ranges between Callovian to Bathonian [*Bill et al.*, 1997; *Schaltegger et al.*, 2002].

7.5. A Conceptual Model to Account for Extreme Crustal Thinning (Figure 14)

[54] Three major structures that were all active during early Jurassic rifting can be identified between the proximal and distal Adriatic rifted margin: the Eita shear zone, the Grosina detachment, and the Pogallo shear zone (Figure 14). Because the Grosina detachment was only active in the brittle crust and the Pogallo shear zone at deeper crustal levels [e.g., *Handy*, 1987], we assume that these structures soled out at in a decollement horizon in the ductile middle crust. Based on this evidence, we interpret that crustal thinning is accommodated by a system of conjugate crustal scale

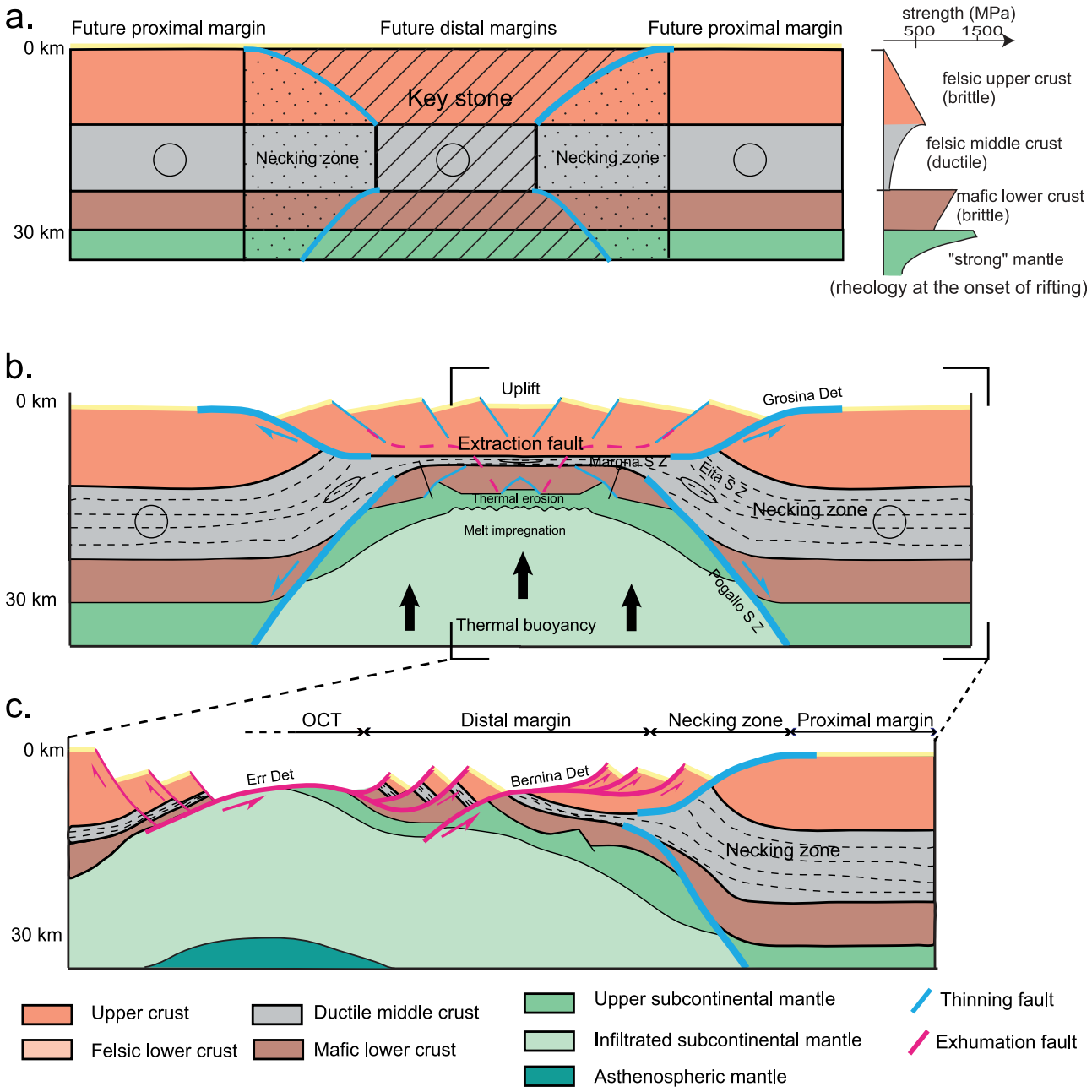

Figure 14. Strain distribution and strain partitioning during lithospheric thinning: (a) exhumation phase, (b) thinning phase, and (c) initial stage. For a discussion see text.

shear zones that are active in the upper brittle crust (e.g., Grosina detachment fault) and in the mafic lower crust and upper mantle (e.g., Pogallo type shear zone) and are decoupled along mid crustal decollements within the brittle-ductile transition (e.g., Eita shear zone) (Figures 13 and 14). We interpret the Margna shear zone [*Müntener and Hermann*, 2001] as an extraction shear zone/decollement from the necking zone to the distal margin, leading to the omission of the mid-crustal level and the direct juxtaposition of the uppermost and lowermost part of the continental crust in the distal margin (Figures 13 and 14) (e.g., extraction fault of *Froitzheim et al.* [2006]).

[55] The strain evolution, spatial relationships and structures that accommodate crustal thinning are shown in a conceptual way in Figure 14. We assume, based on the constrains presented above, a four layer rheology: (1) a strong felsic upper crust (from 0 to 15 km), (2) a weak felsic middle crust (15–25 km), (3) a strong mafic and felsic lower crust consisting of dry granulite and mafic rocks (25–30 km), and (4) a strong and cold subcontinental mantle. The conceptual model shown in Figure 14 is based on the fact that the mass of the crust needs to be conserved during rifting (problem of restoration of sections). The role of structural inheritance and the initial stretching phase (formation of rift basins during an initial stage of rifting) are neglected in our conceptual model shown in Figure 14.

[56] The onset of thinning occurs when deformation starts to localize within the future distal margin. In Figure 14c, this

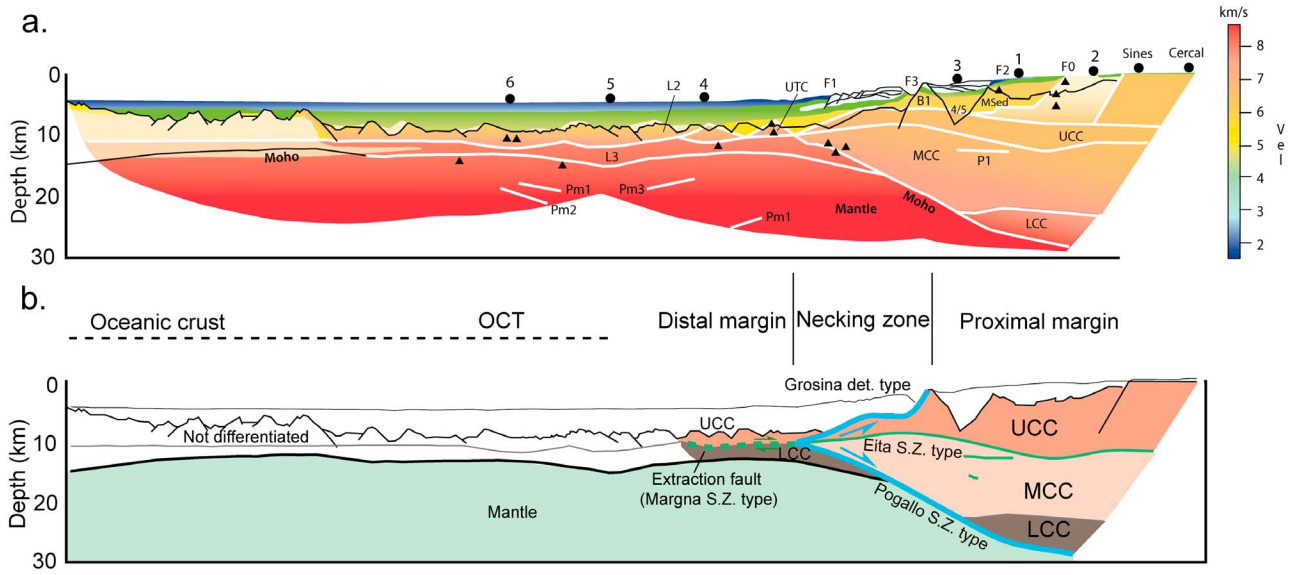

Figure 15. (a) Refraction seismic section across the West Iberia continental margin at 38°N [after *Afilhado et al.*, 2008]. (b) Comparison of the crustal structure of the West Iberia continental margin (subdivision into upper, middle and lower crust) and the structures defined in this work (UCC, Upper Continental Crust; MCC, Middle Continental Crust; LCC, Lower Continental Crust).

is shown by a conjugate set of shear zones that are in the upper felsic brittle crust. These structures are decoupled in a ductile layer in the felsic middle crust. Extension in the rigid mafic/felsic granulitic lower crust and upper mantle is accommodated along conjugate shear zones. This set of conjugate shear zone forms the limit between the future distal and proximal margins, and defines the necking zones of the two margins.

[57] During subsequent thinning, only the hatched areas (necking zones plus future distal margin) will deform. Crustal thinning is accommodated by conjugate shear zones shown in blue (e.g., Grosina and Pogallo) in the brittle upper and lower crusts. These crustal levels will deform by faulting and block rotation while ductile middle crust will act as a decoupling horizon between the two brittle layers. The importance of decoupling horizons during crustal thinning has been already emphasized by *Brun and Beslier* [1996] from analog modeling. In the ductile middle crust, strain will increase toward the necking zone (see strain ellipsoid in Figure 14) as indicated by the formation of shear zones (e.g., Eita shear zone). On the scale of the crust, strain is accommodated, at this stage, by pure shear deformation. The ductile middle crust within the future distal margin will act as an extraction fault (e.g., Margna shear zone), along which the middle crust will be thinned between the rigid upper and lower crust together with the underlying rigid mantle. The higher strain of the ductile layer in the distal margin is compensated by more brittle deformation in the necking zones. A more complex process is supposed to occur in the mantle. Since extension in the brittle upper mantle results in omission and boudinage of the brittle layers, the space created by extension may be replaced by deeper, hotter impregnated mantle. This process may trigger thermal erosion and could be the cause of the strain localization and uplift of the future distal margin (e.g., key stone, Briançonnais [*Lavier and Manatschal*, 2006; *Mohn et al.*, 2010]) during crustal/lithospheric thinning (for more discussion see *Piccardo* [2008] and *Müntener et al.* [2010, and references therein]).

[58] The transition from symmetric thinning to asymmetric exhumation occurs when ductile mid-crustal layers cannot decouple anymore the deformation in the upper crust and mafic lower crust and subcontinental mantle. At this stage, faults can cut from the surface into the mantle and result in the exhumation of mantle rocks in the OCT. These faults (shown in red), are typically downward concave faults that sole out at shallow levels in the mantle and are expressed as low-angle top-basement detachment faults in the distal margin and adjacent OCT (e.g., Bernina and Err detachment faults). During this stage of deformation the former keystone Briançonnais block (or H-block in the terminology of *Lavier and Manatschal*, [2006]) will be delaminated and will form units constituting the final distal margin.

7.6. Implications for Present-Day Rifted Margins (Figure 15)

[59] Interpretation of necking zones at present-day rifted margins remains difficult due to a lack of scientific drill hole data from the basement of the necking zone. In Figure 15, we show the refraction seismic line IAM5 across the Iberia rifted margin [*Afilhado et al.*, 2008]. This line exemplifies the first order crustal structure of many rifted margins. In the IAM5 section (Figure 15a), the Moho as defined by velocities of ~8 km/s is marked by surfaces that can dip up to 35°, corresponding to the necking zone where the crust is thinned from ±30 km to 10 km. Further continentward, in the necking zone, strong sub-horizontal reflections occur, which are clearly within the crust. These reflections are commonly interpreted as "Conrad" reflections, i.e., the contact between upper and lower crust. In the section, mid-crustal velocities are not observed in the most distal margin,

while upper crustal velocities are found directly above a horizon characterized by velocities typical of the lower crust from the proximal margin. Therefore, *Afilhado et al.* [2008] suggested that the middle crust is wedging out toward the necking zone. Restoration of the Adriatic rifted margin (Figure 13) shows many similarities with the refraction seismic data shown in the IAM5 section (Figure 15a) regarding the first-order crustal architecture of the necking zone. We therefore consider that the underlying processes and the strain accommodation within the two margins are comparable. This enables us to propose a structural interpretation of some of the reflections observed in the section in Figure 15b. The Margna-Pogallo shear zone could be linked to the contact between middle crust and mantle that dips continentward. Many authors have proposed that the seismic Moho at the base of the necking zone may correspond to a shear zone [e.g., *Péron-Pinvidic and Manatschal*, 2009]. The apparent dip of the Pogallo shear zone was estimated by *Handy* [1987] between 10° to 34°, which is consistent with observations from present-day margins. The high velocity bodies that seem to be displaced by the Moho could in this case correspond to underplated gabbroic bodies, similar to those observed in the Margna and Ivrea units. The Eita shear zone and associated shear zones in the Campo unit could be equivalents of the reflections within the crust in the IAM5 section (Figure 15a). These reflections are at the top of the middle crust and point oceanward toward the wedge of the middle crust in the necking zone.

[60] The Grosina and Bernina detachments are top-basement detachment faults, locally overlain by extensional allochthons. These structures are therefore not easy to image and interpret in seismic sections [e.g., *Hölker et al.*, 2003]. We suggest, however, that an equivalent structure to the Grosina detachment may occur west of the B1 high (see Figure 15a). This is supported by the observation that the middle crust wedges out in the footwall of this structure and that this structure also separates the distal and proximal margins showing different basin architectures.

[61] The similarity between the structures observed in the Bernina and Campo-Grosina units and those imaged in the IAM5 section (Figure 15a) show that the Alpine analogs represent a valuable natural laboratory to study present-day magma-poor rifted margins, with the significant advantage of allowing us to estimate the age and conditions under which the rift structures formed. Such information is necessary to constrain and test kinematic and dynamic models of rifted-margin formation.

8. Conclusions

[62] In many present-day margins crustal thickness changes abruptly from about 30 km in proximal part to <10 km in hyper-extended domains in the distal part. Such change occurs in a narrow zone, which is referred to as the 'necking zone'. In this paper, we have identified and investigated relics of such a necking zone and its adjacent distal margin preserved in the Campo-Grosina and Bernina units of the Eastern Alps. The study of these units enables us to identify the crustal architecture of the necking zone and to unravel the sedimentary and deformation processes associated with extreme crustal thinning during rifting in the Alpine Tethys margins.

[63] The main conclusions of this study are as follows.

1. The Campo-Grosina units derive from the necking zone of the Adriatic rifted margin. Grosina basement represents a pre-rift upper/middle crust preserving Permian $^{40}Ar/^{39}Ar$ ages in white mica (260.1 ± 2.4 Ma). The Campo unit, instead, consists of pre-rift middle/lower crust, which was exhumed below ~300°C within the necking zone during Pliensbachian time (184.55 ± 1.22 Ma and 188.67 ± 0.86 Ma for $^{40}Ar/^{39}Ar$ ages from biotite) when rifting started to localize within the future distal margin.

2. The Eita shear zone, which marks the contact between the Campo-Grosina units, is interpreted as a decollement/decoupling horizon active at mid-crustal depth within the necking zone at 183–205 Ma, as indicated by $^{40}Ar/^{39}Ar$ ages from white mica and biotite.

3. Thinning in the necking zone is the result of the interplay between detachment faulting in the brittle layers (e.g., Grosina detachment in the upper crust and Pogallo-type shear zone in the lower brittle crust) and decoupling and thinning in ductile quartzo-feldspatic middle and lower crustal levels along localized ductile decollements (e.g., Eita shear zone).

4. The Bernina-Margna units derived from the distal margin, where pre-rift upper crust is juxtaposed against pre-rift lower crust along a major "extraction fault" (e.g., Margna shear zone) responsible for extreme crustal thinning. When the crust is thinned to <10 km, ductile layers become brittle, which enables faults to cut from the surface into the mantle and exhume the brittle crust, as well as the subcontinental mantle, to the seafloor (e.g., Bernina and Err detachments). This process may result in the delamination of the previously thinned hanging wall block (e.g., Briançonnais domain).

[64] These results enable us to propose a coherent structural and tectonic model for the evolution of magma-poor rifted margins during major lithospheric thinning. The necking zone is shown to play a major role in the individualization of the future conjugate continental plates. Furthermore, these symmetric necking zones will define and bound a continental ribbon (also referred to as a key stone block or H-block [*Lavier and Manatschal*, 2006]. Finally this block (e.g., Briançonnais domain) will be delaminated at the end of rifting by low-angle top-basement detachment faulting leading to the exhumation of crustal and subcontinental mantle in the distal margin and adjacent OCT. This final stage will give the large-scale asymmetry observed in many rifted margins.

[65] New structural and thermochronological data of the Adriatic rifted margins enable us to propose a coherent evolution for rifting in Alpine Tethys margin in order to explain major crustal thinning. We believe that these results will help to better understand margins undergoing extreme thinning as well as to constrain and test rift models.

[66] **Acknowledgments.** This manuscript benefited from the thoughtful and constructive reviews of Neil Mancktelow and Yves Lagabielle. We thank Othmar Müntener, Anne-Marie Karpoff, Karel Schulmann, Per Terje Osmundsen, Nikolaus Froitzheim, Richard Corfield, and Patrick Unternehr for helpful discussions. Richard Spikings from the Geneva Isotope Geochronology Laboratory and Terry Spell from Nevada Isotope Geochronology Laboratory are kindly thanked for performing the Ar/Ar thermochronology analysis. This research was financed by the Margin Modeling Phase 2 (MM2) partners (BP, ConocoPhillips, Statoil Hydro, Shell, Petrobras, TOTAL, BG, BHP-Billiton). B. Lehmann is thanked for help in the field, and A. Bouzeghaia is thanked for improving the quality of the figures.

References

Afilhado, A., L. Matias, H. Shiobara, A. Hirn, L. Mendes-Victor, and H. Shimamura (2008), From unthinned continent to ocean: The deep structure of the West Iberia passive continental margin at 38°N, *Tectonophysics*, *458*, 9–50, doi:10.1016/j.tecto.2008.03.002.

Aslanian, D., et al. (2009), Brazilian and African passive margins of the Central Segment of the South Atlantic Ocean: Kinematic constraints, *Tectonophysics*, *468*, 98–112, doi:10.1016/j.tecto.2008.12.016.

Bache, F., J. L. Olivet, C. Gorini, D. Aslanian, C. Labails, and M. Rabineau (2010), Evolution of rifted continental margins: The case of the Gulf of Lions (Western Mediterranean Basin), *Earth Planet. Sci. Lett.*, *292*, 345–356, doi:10.1016/j.epsl.2010.02.001.

Baumgartner, P. O. (1987), Age and genesis of Tethyan Jurassic Radiolarites, *Eclogae Geol. Helv.*, *80*, 831–879.

Beltrando, M., R. Compagnoni, and B. Lombardo (2010), (Ultra-) High-pressure metamorphism and orogenesis: An Alpine perspective, *Gondwana Res.*, *18*, 147–166, doi:10.1016/j.gr.2010.01.009.

Bernoulli, D. (1964), Zur Geologie des Monte Generoso (Lombardische Alpen), *Beitr. Geol. Karte Schweiz*, *118*, 1–134.

Bernoulli, D., G. Bertotti, and N. Froitzheim (1990), Mesozoic faults and associated sediments in the Austro-Alpine-South Alpine passive continental margin, *Mem. Soc. Geol. Ital.*, *45*, 25–38.

Bertotti, G. (1991), Early Mesozoic extension and Alpine shortening in the western southern Alps: The geology of the area between Lugano and Menaggio (Lombardy, northern Italy), *Mem. Sci. Geol.*, *43*, 17–123.

Bertotti, G., V. Picotti, D. Bernoulli, and A. Castellarin (1993), From rifting to drifting: Tectonic evolution of the South-Alpine upper crust from the Triassic to the Early Cretaceous, *Sediment. Geol.*, *86*, 53–76, doi:10.1016/0037-0738(93)90133-P.

Bill, M., F. Bussy, M. Cosca, H. Masson, and J. C. Hunziker (1997), High-precision U-Pb and 40Ar/39Ar dating of an Alpine ophiolite (Gets nappe, French Alps), *Eclogae Geol. Helv.*, *90*, 43–54.

Bissig, T., and J. Hermann (1999), From pre-Alpine extension to Alpine convergence: The example of the southwestern margin of the Margna nappe (Val Malenco, N-Italy), *Schweiz. Mineral. Petrogr. Mitt.*, *79*, 363–380.

Bonsignore, G., A. Borgo, R. Gelati, A. Montrasio, R. Potenza, U. Ragni, and G. Schiavianto (1969), Note illustrative della Carta Geologica d'Italia, Foglio 8-Bormio, Serv. Geol. Ital., Rome.

Boriani, A. C., and I. M. Villa (1997), Geochronology of regional metamorphism in the Ivrea-Verbano Zone and Serie dei Laghi, Italian Alps, *Schweiz. Mineral. Petrogr. Mitt.*, *77*, 381–401.

Braga, R., F. Giacomini, B. Messiga, and R. Tribuzio (2001), The Sondalo Gabbroic complex (Central Alps, Northern Italy): Evidence for emplacement of mantle-derived melts into amphibolite-facies metapelites, *Phys. Chem. Earth Part A*, *26*, 333–342, doi:10.1016/S1464-1895(01)00063-1.

Braga, R., A. Callegari, B. Messiga, L. Ottolini, M. R. Renna, and R. Tribuzio (2003), Origin of prismatine from the Sondalo granulites (Central Alps, northern Italy), *Eur. J. Mineral.*, *15*, 393–400, doi:10.1127/0935-1221/2003/0015-0393.

Brun, J. P., and M. O. Beslier (1996), Mantle exhumation at passive margins, *Earth Planet. Sci. Lett.*, *142*, 161–173, doi:10.1016/0012-821X(96)00080-5.

Bucher, K., and M. Frey (1994), *Petrogenesis of Metamorphic Rocks*, 6th ed., Springer, Berlin.

Bullock, A. D., and T. A. Minshull (2005), From continental extension to seafloor spreading: Crustal structure of the Goban Spur rifted margin, southwest of the UK, *Geophys. J. Int.*, *163*, 527–546, doi:10.1111/j.1365-246X.2005.02726.x.

Cannat, M., G. Manatschal, D. Sauter, and G. Péron-Pinvidic (2009), Assessing the conditions of continental breakup at magma-poor rifted margins: What can we learn from slow spreading mid-ocean ridges?, *C. R. Geosci.*, *341*, 406–427, doi:10.1016/j.crte.2009.01.005.

Chevalier, F., M. Guiraud, J. P. Garcia, J. L. Dommergues, D. Quesne, P. Allemand, and T. Dumont (2003), Calculating the long-term displacement rates of a normal fault from the high-resolution stratigraphic record (early Tethyan rifting, French Alps), *Terra Nova*, *15*, 410–416, doi:10.1046/j.1365-3121.2003.00508.x.

Conti, P., G. Manatschal, and M. Pfister (1994), Synrift sedimentation, Jurassic and Alpine tectonics in the central Ortler Nappe, (Eastern Alps, Italy), *Eclogae Geol. Helv.*, *87*, 63–90.

Contrucci, I., F. Klingelhöfer, J. Perrot, R. Bartolome, M. A. Gutscher, M. Sahabi, J. Malod, and J. P. Rehault (2004a), The crustal structure of the NW Moroccan continental margin from wide-angle and reflection seismic data, *Geophys. J. Int.*, *159*, 117–128, doi:10.1111/j.1365-246X.2004.02391.x.

Contrucci, I., L. Matias, M. Moulin, L. Géli, F. Klingelhofer, H. Nouzé, D. Aslanian, J. L. Olivet, J. P. Réhault, and J. C. Sibuet (2004b), Deep structure of the West African continental margin (Congo, Zaïre, Angola), between 5°S and 8°S, from reflection/refraction seismics and gravity data, *Geophys. J. Int.*, *158*, 529–553, doi:10.1111/j.1365-246X.2004.02303.x.

Cowie, P. A., J. R. Underhill, M. D. Behn, J. Lin, and C. E. Gill (2005), Spatio-temporal evolution of strain accumulation derived from multi-scale observations of Late Jurassic rifting in the northern North Sea: A critical test of models for lithospheric extension, *Earth Planet. Sci. Lett.*, *234*, 401–419, doi:10.1016/j.epsl.2005.01.039.

Dean, S. M., T. A. Minshull, R. B. Whitmarsh, and K. E. Louden (2000), Deep structure of the ocean-continent transition in the southern Iberia Abyssal Plain from seismic refraction profiles: The IAM-9 transect at 40°20′N, *J. Geophys. Res.*, *105*, 5859–5885, doi:10.1029/1999JB900301.

Del Moro, A., and A. Notarpietro (1987), Rb-Sr geochemistry of some Hercynian granitoids overprinted by eo-Alpine metamorphism in the Upper Valtellina, Central Alps, *Schweiz. Mineral. Petrogr. Mitt.*, *67*, 295–306.

Di Vincenzo, G., C. Viti, and S. Rocchi (2003), The effect of chlorite interlayering on 40Ar-39Ar biotite dating: An 40Ar-39Ar laser-probe and TEM investigations of variably chloritised biotites, *Contrib. Mineral. Petrol.*, *145*, 643–658, doi:10.1007/s00410-003-0472-z.

Driscoll, N. W., and G. D. Karner (1998), Lower crustal extension across the Northern Carnarvon basin, Australia: Evidence for an eastward dipping detachment, *J. Geophys. Res.*, *103*, 4975–4991, doi:10.1029/97JB03295.

Eberli, G. P. (1988), The evolution of the Southern Continental Margin of the Jurassic Tethys Ocean as recorded in the Allgau Formation of the Austroalpine Nappes of Graubunden (Switzerland), *Eclogae Geol. Helv.*, *81*, 175–214.

Fernàndez, M., C. Ayala, M. Torne, J. Vergés, M. Gomez, and R. Karpus (2005), Lithospheric structure of the Mid-Norwegian Margin: Comparison between the Møre and Vøring margins, *J. Geol. Soc.*, *162*, 1005–1012, doi:10.1144/0016-764904-116.

Ferrando, S., D. Bernoulli, and R. Compagnoni (2004), The Canavese zone (internal Western Alps): A distal margin of Adria, *Schweiz. Mineral. Petrogr. Mitt.*, *84*(3), 237–256.

Ferreiro Mählmann, R. (1996), The pattern of diagenesis and metamorphism by vitrinite reflectance and illite "crystallinity" in mittelbünden and in the oberhalbstein: Part 2: Correlation of coal petrographical and of mineralogical parameters, *Schweiz. Mineral. Petrogr. Mitt.*, *76*, 23–46.

Finger, W. (1978), Die Zone von Samaden (Unterostalpine Decken, Graubünden) und ihre jurassischen Brekzien, *Mitt. Geol. Inst. Eidg. Tech. Hochsch. Univ. Zurich*, *224*, 1–140.

Froitzheim, N. (1988), Synsedimentary and synorogenic normal faults within a thrust sheet of the Eastern Alps (Ortler zone, Graubunden, Switzerland), *Eclogae Geol. Helv.*, *81*, 593–610.

Froitzheim, N., and G. P. Eberli (1990), Extensional detachment faulting in the evolution of a Tethys passive continental margin, Eastern Alps, Switzerland, *Geol. Soc. Am. Bull.*, *102*, 1297–1308, doi:10.1130/0016-7606(1990)102<1297:EDFITE>2.3.CO;2.

Froitzheim, N., and G. Manatschal (1996), Kinematics of Jurassic rifting, mantle exhumation, and passive-margin formation in the Austroalpine and Penninic nappes (eastern Switzerland), *Geol. Soc. Am. Bull.*, *108*, 1120–1133, doi:10.1130/0016-7606(1996)108<1120:KOJRME>2.3.CO;2.

Froitzheim, N., S. M. Schmid, and P. Conti (1994), Repeated change from crustal shortening to orogen-parallel extension in the Austroalpine units of Graubunden, *Eclogae Geol. Helv.*, *87*, 559–612.

Froitzheim, N., J. Pleuger, and T. J. Nagel (2006), Extraction faults, *J. Struct. Geol.*, *28*, 1388–1395, doi:10.1016/j.jsg.2006.05.002.

Funck, T., J. R. Hopper, H. C. Larsen, K. E. Louden, B. E. Tucholke, and W. S. Holbrook (2003), Crustal structure of the ocean-continent transition at Flemish Cap: Seismic refraction results, *J. Geophys. Res.*, *108*(B11), 2531, doi:10.1029/2003JB002434.

Funck, T., H. R. Jackson, K. E. Louden, S. A. Dehler, and Y. Wu (2004), Crustal structure of the northern Nova Scotia rifted continental margin (eastern Canada), *J. Geophys. Res.*, *109*, B09102, doi:10.1029/2004JB003008.

Furrer, H., B. Aemissegger, G. Eberli, U. Eichenberger, S. Frank, H. Naef, and R. Trümpy (1985), Field workshop on Triassic and Jurassic sediments in the eastern Alps of Switzerland, *Mitt. Geol. Inst. Eidg. Tech. Hochsch. Univ. Zurich*, *248*, 1–81.

Guntli, P., and M. Liniger (1989), Metmorphose in der Margan-Decke im Bereich Piz da la Margna und Piz Fedoz (Oberengadin), *Schweiz. Mineral. Petrogr. Mitt.*, *69*, 289–301.

Handy, M. R. (1987), The structure, age and kinematics of the Pogallo fault zone, southern Alps, northwestern Italy, *Eclogae Geol. Helv.*, *80*, 593–632.

Handy, M. R., and A. Zingg (1991), The tectonic and rheological evolution of an attenuated cross section of the continental crust: Ivrea crustal section, southern Alps, northwestern Italy and southern Switzerland,

Geol. Soc. Am. Bull., *103*, 236–253, doi:10.1130/0016-7606(1991)103<0236:TTAREO>2.3.CO;2.

Handy, M. R., L. Franz, F. Heller, B. Janott, and R. Zurbriggen (1999), Multistage accretion and exhumation of the continental crust (Ivrea crustal section, Italy and Switzerland), *Tectonics*, *18*, 1154–1177, doi:10.1029/1999TC900034.

Hanson, G. N., M. R. El Tahlawi, and W. Weber (1966), KAr and RbSr ages of pegmatites in the south central Alps, *Earth Planet. Sci. Lett.*, *1*, 407–413, doi:10.1016/0012-821X(66)90037-9.

Harrison, T. M., I. Duncan, and I. McDougall (1985), Diffusion of ^{40}Ar in biotite: Temperature, pressure and compositional effects, *Geochim. Cosmochim. Acta*, *49*, 2461–2468, doi:10.1016/0016-7037(85)90246-7.

Harrison, T. M., J. Célérier, A. B. Aikman, J. Hermann, and M. T. Heizler (2009), Diffusion of ^{40}Ar in muscovite, *Geochim. Cosmochim. Acta*, *73*, 1039–1051, doi:10.1016/j.gca.2008.09.038.

Hermann, J., and O. Müntener (1996), Extension-related structures in the Malenco-Margna-system: Implications for paleogeography and consequences for rifting and Alpine tectonics, *Schweiz. Mineral. Petrogr. Mitt.*, *76*, 501–519.

Hermann, J., O. Müntener, V. Trommsdorff, W. Hansmann, and G. B. Piccardo (1997), Fossil crust-to-mantle transition, Val Malenco (Italian Alps), *J. Geophys. Res.*, *102*, 20,123–20,132, doi:10.1029/97JB01510.

Hölker, A. B., G. Manatschal, K. Holliger, and D. Bernoulli (2003), Tectonic nature and siesmic response of top-basement detachment faults in magma-poor rifted margins, *Tectonics*, *22*(4), 1035, doi:10.1029/2001TC001347.

Jaffal, M., F. Klingelhoefer, L. Matias, F. Teixeira, and M. Amrhar (2009), Crustal structure of the NW Moroccan margin from deep seismic data (SISMAR Cruise), *C. R. Geosci.*, *341*, 495–503, doi:10.1016/j.crte.2009.04.003.

Keen, C. E., and B. de Voogd (1988), The continent-ocean boundary at the rifted margin off eastern Canada: New results from deep seismic reflection studies, *Tectonics*, *7*, 107–124, doi:10.1029/TC007i001p00107.

Klingelhoefer, F., C. Labails, E. Cosquer, S. Rouzo, L. Géli, D. Aslanian, J. L. Olivet, M. Sahabi, H. Nouzé, and P. Unternehr (2009), Crustal structure of the SW-Moroccan margin from wide-angle and reflection seismic data (the DAKHLA experiment) Part A: Wide-angle seismic models, *Tectonophysics*, *468*, 63–82, doi:10.1016/j.tecto.2008.07.022.

Koeing, M. A. (1964), Geologisch-petrographische Untersuchungen im oberen Veltlin, PhD thesis, Univ. of Zürich, Zürich, Switzerland.

Kusznir, N. J., and G. D. Karner (2007), Continental lithospheric thinning and breakup in response to upwelling divergent mantle flow: Application to the Woodlark, Newfoundland and Iberia margins, in *Imaging, Mapping and Modelling Continental Lithosphere Extension and Breakup*, edited by G. D. Karner, G. Manatschal, and L. M. Pinheiro, *Geol. Soc. Spec. Publ.*, *282*, 389–419, doi:10.1144/SP282.16.

Lau, K. W. H., K. E. Louden, S. Deemer, J. Hall, J. R. Hopper, B. E. Tucholke, W. S. Holbrook, and H. Christian Larsen (2006), Crustal structure across the Grand Banks-Newfoundland Basin Continental Margin - II. Results from a seismic reflection profile, *Geophys. J. Int.*, *167*, 157–170, doi:10.1111/j.1365-246X.2006.02989.x.

Lavier, L. L., and G. Manatschal (2006), A mechanism to thin the continental lithosphere at magma-poor margins, *Nature*, *440*, 324–328, doi:10.1038/nature04608.

Lemoine, M., et al. (1986), The continental margin of the Mesozoic Tethys in the Western Alps, *Mar. Pet. Geol.*, *3*, 179–199, doi:10.1016/0264-8172(86)90044-9.

Leroy, S., E. d'Acremont, C. Tiberi, C. Basuyau, J. Autin, F. Lucazeau, and H. Sloan (2010), Recent off-axis volcanism in the eastern Gulf of Aden: Implications for plume-ridge interaction, *Earth Planet. Sci. Lett.*, *293*, 140–153, doi:10.1016/j.epsl.2010.02.036.

Lister, G. S., and G. A. Davis (1989), The origin of metamorphic core complexes and detachment faults formed during Tertiary continental extension in the northern Colorado River region, U.S, *J. Struct. Geol.*, *11*, 65–94, doi:10.1016/0191-8141(89)90036-9.

Lizarralde, D., et al. (2007), Variation in styles of rifting in the Gulf of California, *Nature*, *448*, 466–469, doi:10.1038/nature06035.

Manatschal, G. (1999), Fluid- and reaction-assisted low-angle normal faulting: Evidence from rift-related brittle fault rocks in the Alps (Err Nappe, eastern Switzerland), *J. Struct. Geol.*, *21*, 777–793, doi:10.1016/S0191-8141(99)00069-3.

Manatschal, G. (2004), New models for evolution of magma-poor rifted margins based on a review of data and concepts from West Iberia and the Alps, *Int. J. Earth Sci.*, *93*, 432–466, doi:10.1007/s00531-004-0394-7.

Manatschal, G., and D. Bernoulli (1999), Architecture and tectonic evolution of nonvolcanic margins: Present-day Galicia and ancient Adria, *Tectonics*, *18*, 1099–1119, doi:10.1029/1999TC900041.

Manatschal, G., and P. Nievergelt (1997), A continent-ocean transition recorded in the Err and Platta nappes (Eastern Switzerland), *Eclogae Geol. Helv.*, *90*, 3–27.

Manatschal, G., N. Froitzheim, M. Rubenach, and B. D. Turrin (2001), The role of detachment faulting in the formation of an ocean-continent transition: Insights from the Iberia Abyssal Plain, in *Non-Volcanic Rifting of Continental Margins: A Comparison of Evidence from Land and Sea*, edited by R. C. L. Wilson et al., *Geol. Soc. Spec. Publ.*, *187*, 405–428, doi:10.1144/GSL.SP.2001.187.01.20.

Manatschal, G., O. Müntener, L. L. Lavier, T. A. Minshull, and G. Péron-Pinvidic (2007), Observations from the Alpine Tethys and Iberia-Newfoundland margins pertinent to the interpretation of continental breakup, in *Imaging, Mapping and Modelling Continental Lithosphere Extension and Breakup*, edited by G. D. Karner, G. Manatschal, and L. M. Pinheiro, *Geol. Soc. Spec. Publ.*, *282*, 291–324. doi:10.1144/SP282.14.

Manatschal, G., D. Sauter, A. M. Karpoff, E. Masini, G. Mohn, and Y. Lagabrielle (2011), The Chenaillet Ophiolite in the French/Italian Alps: An ancient analogue for an Oceanic Core Complex?, *Lithos*, *124*, 169–184, doi:10.1016/j.lithos.2010.10.017.

Masini, E., G. Manatschal, G. Mohn, J. F. Ghienne, and F. Lafont (2011), The tectono-sedimentary evolution of a supra-detachment rift basin at a deep-water magma-poor rifted margin: The example of the Samedan Basin preserved in the Err nappe in SE Switzerland, *Basin Res.*, *23*, 652–677, doi:10.1111/j.1365-2117.2011.00509.x.

McKenzie, D. (1978), Some remarks on the development of sedimentary basins, *Earth Planet. Sci. Lett.*, *40*, 25–32, doi:10.1016/0012-821X(78)90071-7.

Meier, A. (2003), The Periadriatic Fault System in Valtellina (N-Italy) and the evolution of the southwestern segment of the Eastern Alps, PhD thesis, ETH Zürich, Zürich, Switzerland.

Mohn, G., G. Manatschal, O. Müntener, M. Beltrando, and E. Masini (2010), Unravelling the interaction between tectonic and sedimentary processes during lithospheric thinning in the Alpine Tethys margins, *Int. J. Earth Sci.*, *99*, 75–101, doi:10.1007/s00531-010-0566-6.

Mohn, G., G. Manatschal, E. Masini, and O. Müntener (2011), Rift-related inheritance in orogens: A case study from the Austroalpine nappes in Central Alps (SE-Switzerland and N-Italy), *Int. J. Earth Sci.*, *100*, 937–961, doi:10.1007/s00531-010-0630-2.

Montrasio, A., et al. (1969), Carta geologica d'Italia, foglio 19, Tirano, scale 1:100000, Serv. Geol. Ital., Rome.

Moulin, M., D. Aslanian, J. L. Olivet, I. Contrucci, L. Matias, L. Géli, F. Klingelhoefer, H. Nouzé, J. P. Réhault, and P. Unternehr (2005), Geological constraints on the evolution of the Angolan margin based on reflection and refraction seismic data (ZaïAngo project), *Geophys. J. Int.*, *162*, 793–810, doi:10.1111/j.1365-246X.2005.02668.x.

Mulch, A., M. Cosca, and M. Handy (2002), In-situ UV-laser 40Ar/39Ar geochronology of a micaceous mylonite: An example of defect-enhanced argon loss, *Contrib. Mineral. Petrol.*, *142*, 738–752, doi:10.1007/s00410-001-0325-6.

Müntener, O., and J. Hermann (2001), The role of lower crust and continental upper mantle during formation of non-volcanic passive margins: Evidence from the Alps, in *Non-Volcanic Rifting of Continental Margins: A Comparison of Evidence from Land and Sea*, edited by R. C. L. Wilson et al., *Geol. Soc. Spec. Publ.*, *187*, 267–288, doi:10.1144/GSL.SP.2001.187.01.13.

Müntener, O., J. Hermann, and V. Trommsdorff (2000), Cooling history and exhumation of lower-crustal granulite and upper mantle (Malenco, Eastern Central Alps), *J. Petrol.*, *41*, 175–200, doi:10.1093/petrology/41.2.175.

Müntener, O., G. Manatschal, L. Desmurs, and T. Pettke (2010), Plagioclase peridotites in ocean-continent transitions: Refertilized mantle domains generated by melt stagnation in the shallow mantle lithosphere, *J. Petrol.*, *51*, 255–294, doi:10.1093/petrology/egp087.

Notarpietro, A., and L. Gorla (1981), Contributo alla conoscenza delle formazioni austridiche nell'alta e media Valtellina., *Variazioni petrochimiche nella Formazione di Valle Grosina*, *Bull. Mineral. Rend. Soc. Ital. Mineral. Petrol.*, *37*(2), 755–791.

Olafsson, I., E. Sundvor, O. Eldholm, and K. Grue (1992), Møre Margin: Crustal structure from analysis of Expanded Spread Profiles, *Mar. Geophys. Res.*, *14*, 137–162, doi:10.1007/BF01204284.

Osmundsen, P. T., and J. Ebbing (2008), Styles of extension offshore mid-Norway and implications for mechanisms of crustal thinning at passive margins, *Tectonics*, *27*, TC6016, doi:10.1029/2007TC002242.

Pérez-Gussinyé, M., and T. J. Reston (2001), Rheological evolution during extension at nonvolcanic rifted margins: Onset of serpentinization and development of detachments leading to continental breakup, *J. Geophys. Res.*, *106*, 3961–3975, doi:10.1029/2000JB900325.

Péron-Pinvidic, G., and G. Manatschal (2009), The final rifting evolution at deep magma-poor passive margins from Iberia-Newfoundland: A new

point of view, *Int. J. Earth Sci.*, *98*, 1581–1597, doi:10.1007/s00531-008-0337-9.

Piccardo, G. B. (2008), The Jurassic Ligurian Tethys, a fossil ultraslow-spreading ocean: The mantle perspective, in *Metasomatism in Oceanic and Continental Lithospheric Mantle*, edited by M. Coltorti and M. Gregoire, *Geol. Soc. Spec. Publ.*, *293*, 11–34, doi:10.1144/SP293.2.

Rebay, G., and M. I. Spalla (2001), Emplacement at granulite facies conditions of the Sesia-Lanzo metagabbros: An early record of Permian rifting?, *Lithos*, *58*, 85–104, doi:10.1016/S0024-4937(01)00046-9.

Reston, T. J. (2007), The formation of non-volcanic rifted margins by the progressive extension of the lithosphere: The example of the West Iberian margin, in *Imaging, Mapping and Modelling Continental Lithosphere Extension and Breakup*, edited by G. D. Karner, G. Manatschal, and L. M. Pinheiro, *Geol. Soc. Spec. Publ.*, *282*, 77–110, doi:10.1144/SP282.5.

Reston, T. J. (2009), The structure, evolution and symmetry of the magma-poor rifted margins of the North and Central Atlantic: A synthesis, *Tectonophysics*, *468*, 6–27, doi:10.1016/j.tecto.2008.09.002.

Ricou, L. E. (1994), Tethys reconstructed: Plates, continental fragments and their boundaries since 260 Ma from Central America to South-eastern Asia, *Geodin. Acta*, *7*, 169–218.

Schaltegger, U., L. Desmurs, G. Manatschal, O. Müntener, M. Meier, M. Frank, and D. Bernoulli (2002), The transition from rifting to sea-floor spreading within a magma-poor rifted margin: Field and isotopic constraints, *Terra Nova*, *14*, 156–162, doi:10.1046/j.1365-3121.2002.00406.x.

Schmid, S. M., O. A. Pfiffner, N. Froitzheim, G. Schönborn, and E. Kissling (1996), Geophysical-geological transect and tectonic evolution of the Swiss-Italian Alps, *Tectonics*, *15*, 1036–1064, doi:10.1029/96TC00433.

Schmid, S. M., B. Fügenschuh, E. Kissling, and R. Schuster (2004), Tectonic map and overall architecture of the Alpine orogen, *Eclogae Geol. Helv.*, *97*, 93–117, doi:10.1007/s00015-004-1113-x.

Schudel, W. (1965), Geologie der Val Grosina, Provinz Sondrio, Italia, PhD thesis, ETH Zürich, Zürich, Switzerland.

Schüpbach, M. A. (1974), Comparison of slope and basinal sediments of a marginal cratonic basin (Pedregosa Basin, New Mexico) and a marginal geosynclinal basin (Southern border of Piemontais Geosyncline, Bernina nappe, Switzerland), PhD thesis, Rice Univ., Houston, Tex.

Schuster, R., and K. Stüwe (2008), Permian metamorphic event in the Alps, *Geology*, *36*, 603–606, doi:10.1130/G24703A.1.

Sibuet, J. C. (1992), New constraints on the formation of the non-volcanic continental Galicia-Flemish Cap conjugate margins, *J. Geol. Soc.*, *149*, 829–840, doi:10.1144/gsjgs.149.5.0829.

Sölva, H., M. Thöni, and G. Habler (2003), Dating a single garnet crystal with very high Sm/Nd ratios (Campo basement unit, Eastern Alps), *Eur. J. Mineral.*, *15*, 35–42, doi:10.1127/0935-1221/2003/0015-0035.

Spillmann, P., and H. J. Büchi (1993), The Pre-Alpine Basement of the Lower Austroalpine Nappes in the Bernina Massif (Grisons, Switzerland; Valtellina, Italy), in *The Pre-Mesozoic Geology in the Alps*, edited by J. F. von Raumer and F. Neubauer, pp. 457–467, Springer, Berlin, doi:10.1007/978-3-642-84640-3_27.

Staub, R. (1946), Geologische Karte der Berninagruppe und ihrer Umgebung im Oberengadin, Bergell, Val Malenco, Puschlav und Livigno, scale 1:50,000, *Spez. Karte 118*, Geol. Komm., Wabern, Switzerland.

Stipp, M., H. Stünitz, R. Heilbronner, and S. M. Schmid (2002), The eastern Tonale fault zone: A 'natural laboratory' for crystal plastic deformation of quartz over a temperature range from 250 to 700°C, *J. Struct. Geol.*, *24*, 1861–1884, doi:10.1016/S0191-8141(02)00035-4.

Thinon, I., J. P. Réhault, and L. Fidalgo-González (2002), The syn-rift sedimentary cover of the North Biscay Margin (bay of Biscay): From new reflection seismic data, *Bull. Soc. Geol. Fr.*, *173*, 515–522, doi:10.2113/173.6.515.

Thinon, I., L. Matias, J. P. Réhault, A. Hirn, L. Fidalgo-González, and F. Avedik (2003), Deep structure of the Armorican Basin (Bay of Biscay): A review of Norgasis seismic reflection and refraction data, *J. Geol. Soc.*, *160*, 99–116, doi:10.1144/0016-764901-103.

Thöni, M. (1981), Degree and evolution of the alpine metamorphism in the Austroalpine unit W of the Hohe Tauern in the light of K/Ar and Rb/Sr age determinations on micas, *Jahrb. Geol. Bundesanst.*, *131*, 169–201.

Thöni, M. (1999), A review of geochronological data from the Eastern Alps, *Schweiz. Mineral. Petrogr. Mitt.*, *79*, 209–230.

Tribuzio, R., M. F. Thirlwall, and B. Messiga (1999), Petrology, mineral and isotope geochemistry of the Sondalo gabbroic complex (Central Alps, Northern Italy): Implications for the origin of post-Variscan magmatism, *Contrib. Mineral. Petrol.*, *136*, 48–62, doi:10.1007/s004100050523.

Van Avendonk, H. J. A., W. S. Holbrook, G. T. Nunes, D. J. Shillington, B. E. Tucholke, K. E. Louden, H. C. Larsen, and J. R. Hopper (2006), Seismic velocity structure of the rifted margin of the eastern Grand Banks of Newfoundland, Canada, *J. Geophys. Res.*, *111*, B11404, doi:10.1029/2005JB004156.

von Quadt, A., M. Grunenfelder, and H. Buchi (1994), U-Pb zircon ages from igneous rocks of the Bernina nappe system (Grisons, Switzerland), *Schweiz. Mineral. Petrogr. Mitt.*, *74*, 373–382.

Whitmarsh, R. B., R. S. White, S. J. Horsefield, J. C. Sibuet, M. Recq, and V. Louvel (1996), The ocean-continent boundary off the western continental margin of Iberia: Crustal structure west of Galicia Bank, *J. Geophys. Res.*, *101*, 28,291–28,314, doi:10.1029/96JB02579.

Whitmarsh, R. B., G. Manatschal, and T. A. Minshull (2001), Evolution of magma-poor continental margins from rifting to seafloor spreading, *Nature*, *413*, 150–154, doi:10.1038/35093085.

Zelt, C. A., K. Sain, J. V. Naumenko, and D. S. Sawyer (2003), Assessment of crustal velocity models using seismic refraction and reflection tomography, *Geophys. J. Int.*, *153*, 609–626, doi:10.1046/j.1365-246X.2003.01919.x.

M. Beltrando, CNR-IGG, Via Valperga Caluso 35, I-10125 Torino, Italy.

N. Kusznir, Department of Earth and Ocean Sciences, University of Liverpool, 4 Brownlow St., Liverpool L69 3GP, UK.

G. Manatschal, E. Masini, and G. Mohn, CNRS-EOST, Université de Strasbourg, 1 rue Blessig, F-67084 Strasbourg, France. (geoffroy.mohn@eost.u-strasbg.fr)